TERRAIN PROFILE ESTIMATION OVER A SYNTHETIC TERRAIN BY USING PULSE-DOPPLER RADAR

A THESIS

SUBMITTED TO THE DEPARTMENT OF ELECTRICAL AND

ELECTRONICS ENGINEERING

AND THE INSTITUTE OF ENGINEERING AND SCIENCES

OF BILKENT UNIVERSITY

IN PARTIAL FULFILLMENT OF THE REQUIREMENTS

FOR THE DEGREE OF

MASTER OF SCIENCE

By

Onur Tan

June 2010

I certify that I have read this thesis and that in my opinion it is fully adequate, in scope and in quality, as a thesis for the degree of Master of Science.

Prof. Dr. Orhan Arıkan (Supervisor)

I certify that I have read this thesis and that in my opinion it is fully adequate, in scope and in quality, as a thesis for the degree of Master of Science.

Asst. Prof. Dr. Sinan Gezici

I certify that I have read this thesis and that in my opinion it is fully adequate, in scope and in quality, as a thesis for the degree of Master of Science.

Asst. Prof. Dr. İbrahim Körpeoğlu

Approved for the Institute of Engineering and Sciences:

Prof. Dr. Mehmet Baray
Director of Institute of Engineering and Sciences

ABSTRACT

TERRAIN PROFILE ESTIMATION OVER A SYNTHETIC TERRAIN BY USING PULSE-DOPPLER RADAR

Onur Tan
M.S. in Electrical and Electronics Engineering
Supervisor: Prof. Dr. Orhan Arıkan
June 2010

The systems used for terrain profile estimation arise when the safety flight issues in civil flight transport and in military applications become important. These systems are developed for the purpose of terrain avoidance and safe flight. In this thesis, we study two techniques in estimating the terrain profile of the synthetically generated terrain which is achieved by means of signal processing. The estimation performance of the techniques is observed according to the results of flight simulations realized on the simulation environment. In the simulations, an aircraft with a pulse-Doppler radar scans a synthetic terrain according to the scanning patterns to generate the received signals. The techniques that we propose, are applied to the output of the pulse-Doppler process. The first technique is based on the usage of the first and the middle reflection range points in the clutter received signal. An adaptive thresholding method is developed for robust detection of these points. Accurate detection of these range points is crucial in the estimation performance of the first approach. The other technique uses the relation between the elevation angle θ and the clutter received signal amplitude

ratio of the two receiver antennas $R1$ and $R2$ in finding the θ angles of the reflections in corresponding range values. In this approach, accurate estimation of the angle of arrival is important on the performance of estimation. Especially for far ranges, the errors in the estimation become more sensitive to the errors in the elevation angle θ. Finally, over a set of synthetically generated terrain profiles, the error performance of these two techniques are investigated and compared.

Keywords: Pulse-Doppler Processing, Fractal Methods, Synthetic Environments, Terrain Maps, Terrain Avoidance, Pulse-Doppler Radars, Detection.

ÖZET

SENTETİK ARAZİ ÜZERİNDE DARBE-DOPPLER RADARI KULLANARAK YAPILAN ARAZİ PROFİLİ KESTİRİMİ

Onur Tan
Elektrik ve Elektronik Mühendisliği Bölümü Yüksek Lisans
Tez Yöneticisi: Prof. Dr. Orhan Arıkan
Haziran 2010

Arazi profili kestirimi için kullanılan sistemler, sivil uçak taşımacılığı ve askeri uygulamalardaki güvenli uçuş meselelerinin önemli hale gelmesiyle baş göstermiştir. Bu sistemler araziden kaçınma ve güvenli uçuş amacıyla geliştirilmiştir. Bu tezde, sentetik olarak oluşturulmuş arazinin sinyal işleme yardımı ile yapılan arazi profili kestiriminde iki teknik üzerinde çalıştık. Simulasyon ortamında gerçekleştirilen uçuş simulasyonlarının sonuçlarına göre, tekniklerin kestirim performansı gözlemlendi. Simulasyonlarda, darbe-Doppler radarlı bir uçak, alıcı sinyallerini oluşturmak için, tarama şekline göre sentetik araziyi tarar. Önerdiğimiz teknikler, darbe-Doppler işlemenin çıktıları üzerinde uygulanmıştır. İlk teknik, yansıma sinyalindeki ilk ve ortanca yansıma mesafe noktalarının kullanılmasına dayanmaktadır. Bu noktaların gürbüz bir şekilde saptanması için bir uyarlanabilir eşikleme methodu geliştirilmiştir. Bu mesafe noktaların hatasız saptanması, ilk yaklaşımın kestirim performansında önemli bir yer kaplar. Diğer teknik, uygun mesafe değerlerindeki yansımaların yükseliş açısını bulmada, θ ile $R1$ ve $R2$ alıcı antenlerinin yansıma sinyalleri büyüklük

oranı arasındaki ilişkiyi kullanır. Bu yaklaşımda, gelme açısının hatasız kestirimi, kestirim performansı üzerinde önemlidir. Özellikle uzak menzillerde, kestirim üzerindeki hatalar, yükseliş açısı θ üzerindeki hatalara daha duyarlı hale gelir. Son olarak, sentetik olarak oluşturulmuş bir takım arazi profilleri üzerinde, bu iki tekniğin hata performansları incelenmiş ve karşılaştırılmıştır.

Anahtar Kelimeler: Darbe-Dopler İşleme, Fraktal Yöntemler, Sentetik Ortamlar, Arazi Haritaları, Araziden Kaçınma, Darbe-Doppler Radarları, Saptama.

ACKNOWLEDGMENTS

I gratefully thank to my supervisor Prof. Dr. Orhan Arıkan for his supervision, suggestions and encouragement throughout the development of this thesis.

I am also indebted to Asst. Prof. Dr. Sinan Gezici and Asst. Prof. Dr. İbrahim Körpeoğlu for accepting to read and review this thesis and for their suggestions.

It's a great pleasure to express my special thanks to my family who brought me to this stage with their endless love, support and encouragement throughout my life.

I would also thank to friends for their help and friendship throughout all these years.

Contents

List of Figures

Aileme

Chapter 1

INTRODUCTION

The systems used in terrain profile estimation have been developed for the purpose of safe flights. During the recent decades, the developments in the technology also brings concerns about the safety issue. In civil transport, in military applications, safe flight became important due to bad crashes resulted such as loss of aircrafts and crews. There are various reasons for crashes such as bad weather conditions, loss of pilot's attention due to relatively featureless desert terrain, etc. So, terrain profile information is needed to help the pilot for safe flight. These systems detect the collision hazards along the flight path and the pilot has been warned to reduce the risk of collision. For example, Ground Proximity Warning System (GPWS) is used to alert the aircraft in civil transport in danger of collision hazard [1]. In vertical situation display (VSD) systems, the generated terrain profile information is displayed throughout a display in front of the pilot [2]. These kinds of systems will be mentioned in chapter 2. There are lots of patents developed in this area of terrain profile generation and display. Radar signal processing techniques are used in the development of the terrain profile estimation.

Radar signal processing is a very wide, wellrounded area used for detection, tracking, imaging, etc [3]. In this thesis, pulse-Doppler radar systems are used for the terrain profile estimation. Pulse-Doppler radar systems specifies the target's position and target's doppler speed according to the radar platform by applying pulse-Doppler processing techniques on the received signals [3, 4]. For our purpose, target signals are the signals reflected from the terrain. In radar literature, these echoes are called clutter.

In this thesis, we study how to estimate the terrain profile of a synthetically generated terrain with optimum error values. Therefore, a simulation environment is created to achieve these goals. Simulation environment basically includes the synthetically generated terrain, transmitted pulse shape parameters and antenna pattern used in the simulations. A realistic synthetic terrain generation is significant in the success of the techniques used in this thesis. So, we investigate many techniques and synthetic terrain is generated realistically as possible as the actual terrain shapes, to get reasonable and good results. In the simulations, basically an aircraft with a pulse-Doppler radar flies over the synthetic terrain. We simulate the aircraft in the simulation environment according to the particular scanning patterns for each technique. The aircraft scans the synthetic terrain by transmitting pulses with its pulse-Doppler radar antenna and it receives the corresponding echoes reflected from the synthetic terrain. These received signals are processed for estimating the terrain profile of the synthetic terrain. In this thesis, we developed two techniques. And these two techniques are based on the processing of the received signals for the terrain profile estimation. As mentioned, they have their own scanning patterns during the simulations. For the simulations, the transmitted pulse shape and the generated synthetic terrain are created at the beginning. Generated synthetic terrain is scanned according to the scanning pattern of these two techniques by transmitting the generated pulses. Then, raw radar data is generated to be used in the generation of the received signals. These received signals are pulse-Doppler processed before applying the two

developed techniques over them. Until obtaining the pulse-Doppler processed received signals, the same steps are applied in the simulations of each technique with their particular scanning patterns. These techniques are applied over the pulse-Doppler processed received signals for the estimation of the terrain profile. First technique is based on the usage of the time of arrival information of the echoes, on the other hand, the other technique is based on the usage of angle of arrival information. Time of arrival information of the echoes are related with the range of the echoes according to the aircraft position for the time of arrival based terrain profiling technique. Angle of arrival information is the elevation angle of the echoes according to the horizon for the angle of arrival based terrain profiling technique. They will be discussed in detail. Finally, we compared and investigated these two developed techniques with their error performances in terrain profile estimation by means of the results of the simulations.

The outline of the thesis is as follows. Chapter 2 includes the related works with the thesis in the literature. In chapter 3, the generation of the elements in the simulation environment is mentioned. Chapter 4 is about two developed techniques used in the terrain profile estimation and the estimation results. Chapter 5 concludes the thesis with a general summary of the results.

Chapter 2

RELATED WORKS

The systems that are in the literature, generally developed for the purpose of the terrain avoidance and safe flight. They aim to detect and warn the collision hazards along the flight path of the aircraft. Through these systems, aircrafts can fly safely in various weather conditions in any time of the day. For example, when flying relatively featureless desert terrain, a desert storm can cause a pilot lose depth perception [5]. In these situations, it's very crucial to show the terrain elevation data in a display in front of the pilot, to prevent from bad results such as loss of aircrafts and crews.

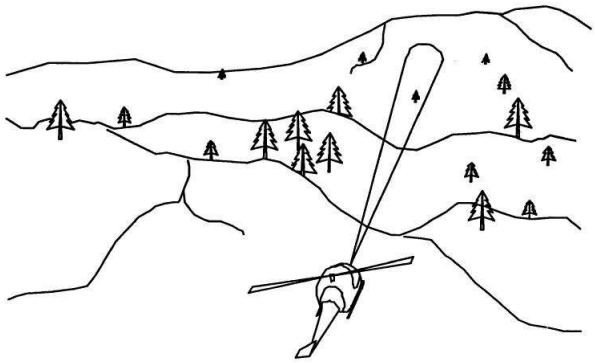

Figure 2.1: Scanning of the terrain with a pencil beam antenna pointed along the flight path.

In the Honeywell Technology Center, a forward looking altimeter for the terrain avoidance is developed. In Fig. 2.1, the terrain is scanned by the aircraft with a pencil beam antenna, to reduce the risk of a collision. For this purpose, the performance of the radar is tested in different terrains for different weather conditions successfully [5]. The system works in the sense of transmitting and receiving pulses. By processing received signals, the terrain profile information is extracted. A pencil beam antenna is used to scan the terrain. Because, it's important to get a good resolution for detecting the terrain easily. By means of this narrow beam, this resolution values can be obtained.

The system is tested successfully in different types of terrains including ground, meadows, wheat fields, etc. It provides accurate information about the low level flying hazards such as trees, poles, buildings. The only problem about the system occurs in rainy weathers. Due to the strong reflections from the rain, sometimes rainy areas can be detected as a hazard [5].

The other system that we come across, is the Ground Proximity Warning System (GPWS). It's generally used in civil flight transport to alert when the aircraft is in danger of impacting terrain [1, 6, 7]. These systems are very important to warn the aircraft against the possible hazards in the landing path.

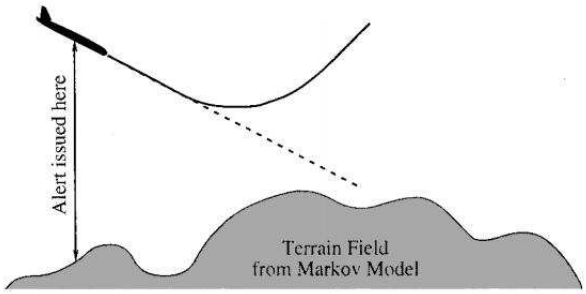

Figure 2.2: The landing of the aircraft.

In Fig. 2.2, alert issued before the terrain field in the landing of the aircraft. The early warnings are very important for the pilot to have some response time. There are flight accidents, involving aircraft with a functioning GPWS. GPWS sometimes couldn't alert due to false alarms. Late warnings, in which pilot has little time to respond, is another reason to these accidents. Lastly, due to the poor pilot responses, these accidents can be occured [1, 6, 7].

Specifically, GPWS can operate by modelling the terrain statistically. The terrain is modelled by using Markov statistic models. The probabilities of an impacting terrain in the flight path are calculated according to these models, and the pilot is warn by an alarm mechanism in case of necessity [1, 8].

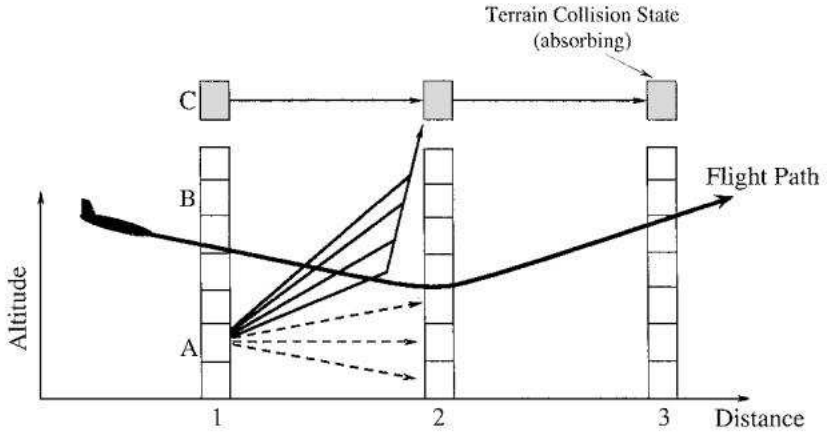

Figure 2.3: The markov chain propagation method.

The procedure for the markov chain propagation, includes tracking the probability that the terrain reaches different altitudes in the flight path. Consider the case in Fig. 2.3 in which the terrain altitude is in state A. The transitions from A to the states above the aircraft's flight path will result in a collision, so these transition probabilities combine to the terrain collision state [1, 8].

For instance, terrain in state B is above the flight path. That's why it directly goes into the terrain collision state. Being in the terrain collision state at each

step, is another way of telling the running probability that a collision with a terrain has occured [1, 8].

There are lots of patents in the literature to provide the safe flight of the aircraft. Through a display, the terrain profile along the flight path is reflected to the pilot to minimize the risk of collision.

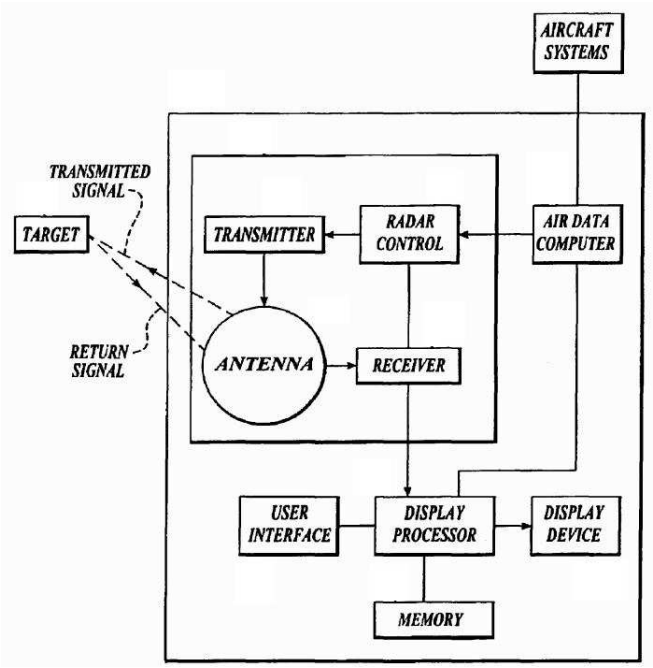

Figure 2.4: The block diagram of the system developed in one of the patent.

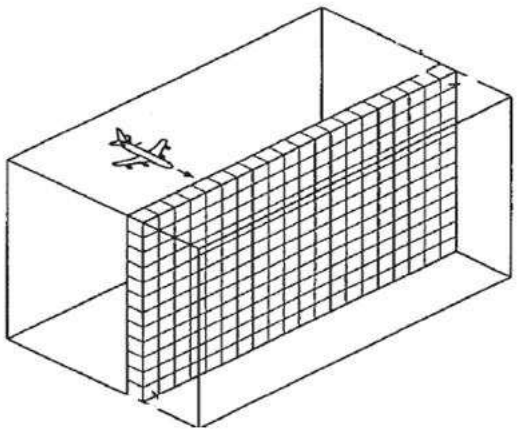

Figure 2.5: Three dimensional buffer.

In Fig. 2.4, the general block diagram of one of the patent is shown. Basically, the system includes a memory, a processor and a display device. It shows the steps that has to be achieved to display the terrain profile for the safe flight. Radar control unite controls the transmitter and receiver. After transmitting the pulses by the antenna, received signals are processed in a format to be stored in a three-dimensional buffer. These processed signals are stored in a plane of voxels in the three-dimensional buffer like in Fig. 2.5. The display device is coupled to the processor for displaying the image [9].

In the patents, there are various ways of displaying the terrain profile for the easy understanding of the pilot. Like in Fig. 2.6, there is a display in front of the pilot showing the profile of the terrain. This terrain display format is crucial for situational awareness of the pilot [10].

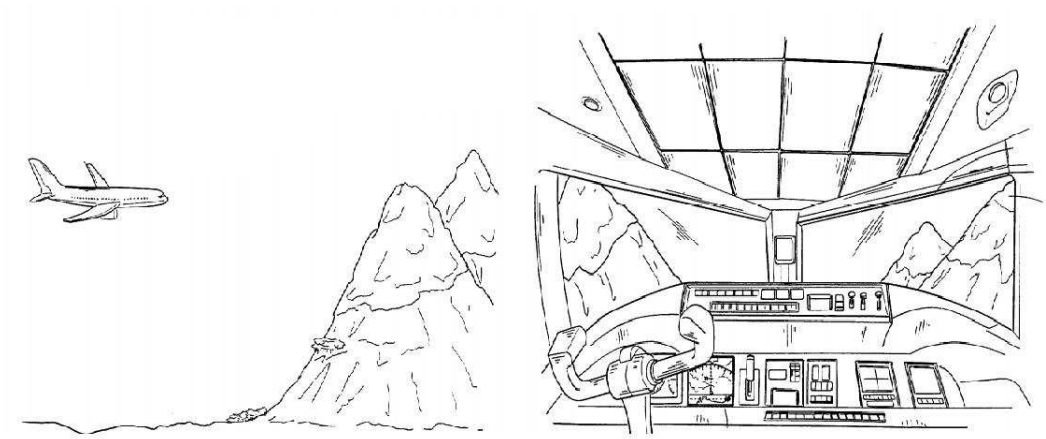

Figure 2.6: The pilot cabin.

A vertical situation display (VSD) provides a two-dimensional representation of an aircraft, the aircraft flight plan and terrain under the aircraft. It simply gives bird's eye view of the terrain under the aircraft. Furthermore, the altitude profile in the horizontal axes to the flight path is shown. In Fig. 2.7, we can see the terrain image generated by VSD system in a flight deck display screen. The relative position and height information of the flight according to the terrain can

be extracted. In this regard, a member of the aircraft crew can easily understand the vertical situation of the aircraft relative to the terrain with a simple glance at the display in Fig. 2.7 [2].

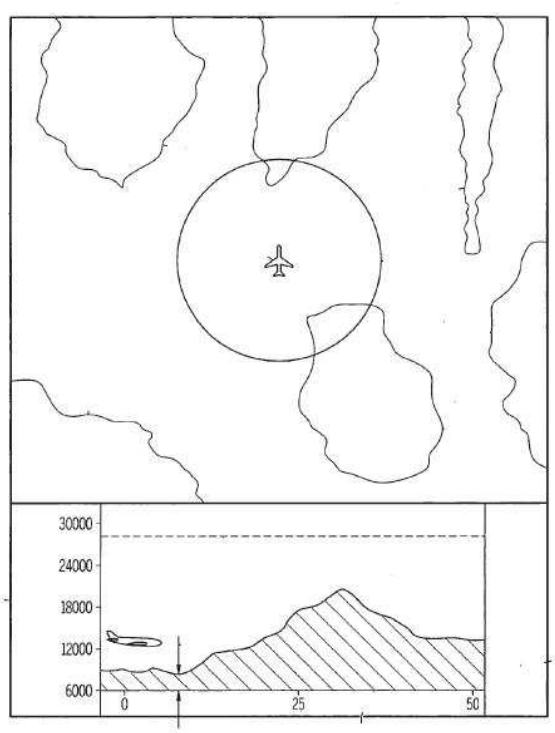

Figure 2.7: The sample terrain image generated by VSD system.

The frequent display of the terrain elevation data in the flight path, is the vertical display image in front of the aircraft as in Fig. 2.8. Vertical front view is the most common display mode that we came across through out the literature [11].

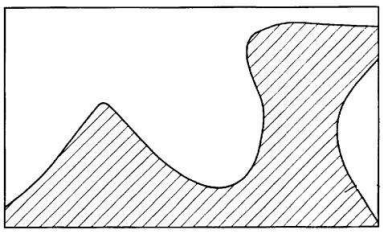

Figure 2.8: Vertical front view.

Fig. 2.9 is a cathode ray tube display, in which it has the contoured terrain elevation in the plan view and a corresponding vertical front view. This is another display mode, showing the terrain elevation under the aircraft as well as aircraft altitude. By means of this display, the relationship between the aircraft and the terrain altitudes can be seen easily [11].

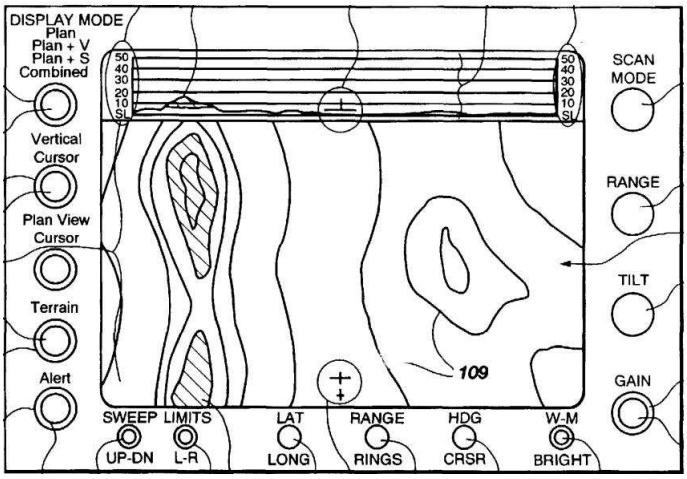

Figure 2.9: The display of contoured terrain data with vertical front view.

To sum up, most of the systems are developed for providing the safe flight of the aircraft. They try to minimize the risk level of collision and warn the pilot to prevent the crashes. For this purpose, GPWS has some alarm mechanism to warn the pilot and crew. The display of the terrain profile is another way of informing the pilot about the terrain elevation along the flight path. Displaying the terrain elevation data in the easiest and useful manner is very important such that the pilot can have a good response. So, there are lots of different display sytles of this data. Briefly, the main aim under these systems is helping the pilot to provide a safe flight.

Chapter 3

SIMULATION ENVIRONMENT

In this chapter, a simulation environment is formed up to run the simulations for the developed techniques. Firstly, a synthetic terrain is needed such that an aircraft can be simulated over it. In the simulation, the aircraft flies on a specific altitude and scans the terrain by transmitting some pulses. Raw radar data is generated as a result of the scans. By using these raw radar data results, received signals are generated such that we can process them to estimate the terrain profile. Briefly, this simulation environment is begun with generating a terrain elevation data which should be realistic as possible as the real terrain shapes. For this purpose, some techniques are investigated and compared so that we can obtain good synthetic terrain results.

3.1 Related Work

There are basically two way of existing terrain generation. These are seperated as, GIS (Geometric Information Systems) and fractal based techniques. In GIS

techniques, elevation data is derived from the real world measurements such as using Satellite Imagery. On the other hand, fractal technique is a procedural way in which the terrain is generated programmatically. It's not easy to access terrain data derived by GIS techniques. Thus, our focus is the fractal techniques, in which the terrain can be generated synthetically.

Terrain generation is the computer representation and display of the natural landscape features. Fractal techniques are used to attempt mimic nature as closely as possible. It's obvious that, there have been a great progress in this area by looking the quality of games, computer graphics and films. So, here comes the question "what's fractal?". A fractal is a complex shape that is produced mathematically with recursion, and it results in an image that each part or whole will look similar to another one. It's a geometric pattern used especially in computer modelling of irregular patterns and structures in nature that can not be represented by classical geometry. In nature, terrains have generally irregular shapes. Therefore, fractal methods are used for generating realistic landscapes and terrain elevation data [12, 13, 14, 15].

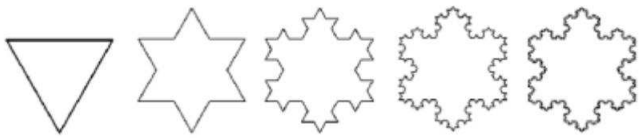

Figure 3.1: Obtaining snowflake by using fractal.

Fig. 3.1 is a simple example of showing what fractal looks like and how it works. It's aimed to get a snowflake shape from starting an equilateral triangle. Basically, the process here is that the equilateral triangle gets repeated for as much iteration as desired to reach a snowflake shape at the end [12].

The key concept of generating fractal terrain is self-similarity. An object is said to be self-similar when magnified subsets of the object look like the whole and

to each other. Terrain is a self-similar object. For example, a jagged edge broken rock in your hand has the same irregularities as the ridgeline on a distant horizon. So, this self-similarity property allows us to use fractals to generate synthetic terrain which still looks like terrain regardless of which scale it's displayed [16, 17, 18]. Let's have a look at the methods for generating synthetic terrains.

3.1.1 Midpoint Displacement In One Dimension

One-dimensional midpoint displacement is an algorithm to draw ridgelines, as mountains appear on a distant horizon. The algorithm begins with a single horizontal line and it repeats for a sufficiently large number of times. The algorithm finds the midpoint of the line segment and replace the midpoint by a random amount. Then, it reduces the range of random numbers. It repeats over this procedure for each line segment. It's easier to understand with an example. Let's take a straight line between -1.0 and 1.0 in x axes. And the random number range is initially set from -1.0 to 1.0. After the first iteration, the line at the top in Fig. 3.2 is obtained. In second iteration, it has two lines that have the same length. Random number range is decreased by half amount to -0.5 to 0.5. For each of the midpoint, a random number is generated in this range and we obtain the line at the middle in Fig. 3.2. Samely after third iteration, the line at the bottom in Fig. 3.2 is obtained. It's an easy example to understand the logic of this algorithm [16].

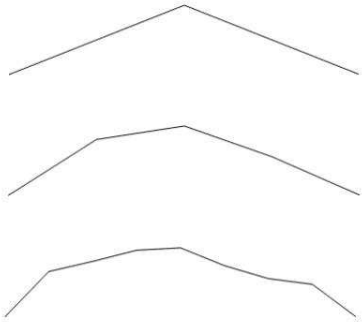

Figure 3.2: An example illustration of midpoint displacement in one dimension with three iteration.

The important point in specifying the roughness of the ridgeline is the parameter H. It is the value which determines how much the random number range is reduced each time through the loop. The range can be reduced in each time through the loop by multiplying it with $H.2^{-H}$. By means of this, it can be determined how jagged or smooth the ridgelines will be. In Fig. 3.3, the effect of H values on the roughness of the ridgelines are shown. With larger H values,the range is reduced more in each loop which is causing smoother ridgelines. With lower H values, the jagged ridgelines can be obtained as seen in Fig. 3.3 [16].

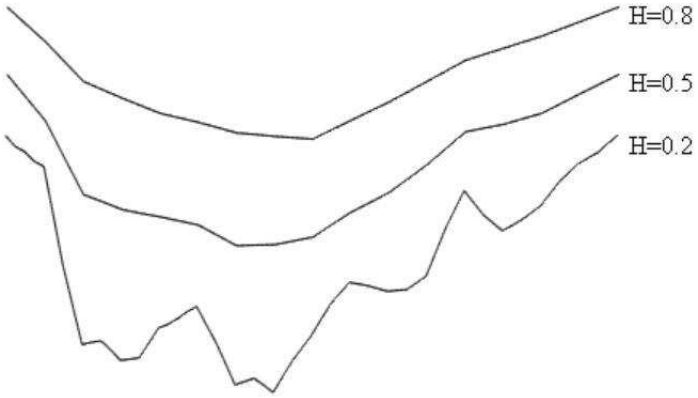

Figure 3.3: The effect of H value on the roughness of the ridgeline.

This is a simple fractal algorithm in one dimension. But it creates very complex result which is the beauty of fractals. It also gives the possibility to create more realistic and detailed images in 2D. Fig. 3.4 is the example of the ridgeline obtained by using this algorithm.

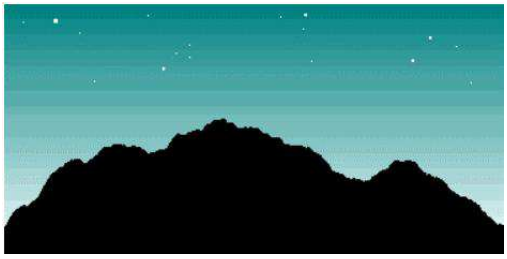

Figure 3.4: The ridgeline obtained by midpoint displacement in one dimension.

3.1.2 Height Maps

A height map is the simplest way of generating a terrain. It's a 2D array of height values. Height maps can be obtained as physical measurements from the actual terrain by Geological Survey from the various parts of the country and used to create authentic landscapes. On the other hand, a height map could be any arbitrary definition of heights. A gray scale image is another example of height maps. Gray scale image is the instance of displaying the height map as an image by assigning a colour to each height value. High points are assigned to white, whilst lowers black in gray scale image. Fig. 3.5 (a) illustrates an image of randomly generated clouds using a computer tool. It can be accomplished by using fractals as well. Fig. 3.5 (b) is the resulting terrain using this gray scale image [19, 20].

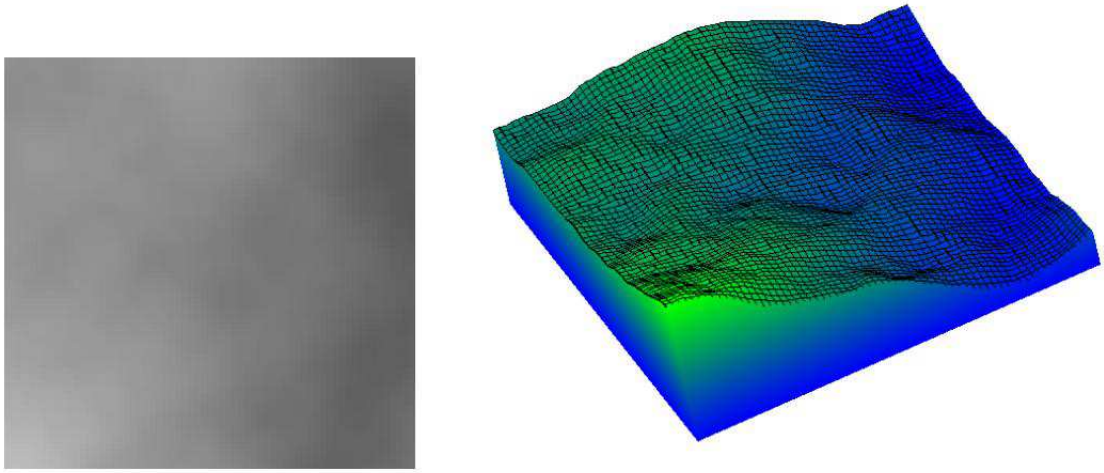

(a) (b)

Figure 3.5: (a) A gray scale image height map; (b) the corresponding landscape generated from the image height map.

3.1.3 Recursive Subdivison Methods

Recursive subdivision methods are based on generating a terrain by recursively subdividing it into smaller pieces. It's begun with the edge grid points defining a square. And the region is subdivided according to the logic of the algorithm until the suitable resolution is achieved. These methods are considered to be a fractal due to the self-similarity property in their construction. In each subdivison, the same logic of the algorithm is carried out. So recursion is inevitable. Also in each subdivision, a random offset is added to the new vertices created. This allows a variation in the terrain. In these methods, unwanted spikes in the new vertices are prevented due to the proportionality. So, by means of these properties in the nature of recursive subdivison methods, more realistic synthetic terrains can be generated [19, 21, 22, 23].

Triangular-Edge Subdivision

It's the simplest subdivision method of generating fractal terrains. It takes each grid as square and logically divides it into two triangles. The midpoint of each triangle's edge is set to a random amount. Fig. 3.6 (a) shows the four initial grid points to begin the algorithm. In Fig. 3.6 (b), the red points are the new midpoint values created after one iteration. These four created smaller squares can be subdivided again. This procedure goes on until all pixels in the matrix are set to a value. Thus, a 2D array indices are filled with height values which becomes a generated fractal terrain [19, 24, 25].

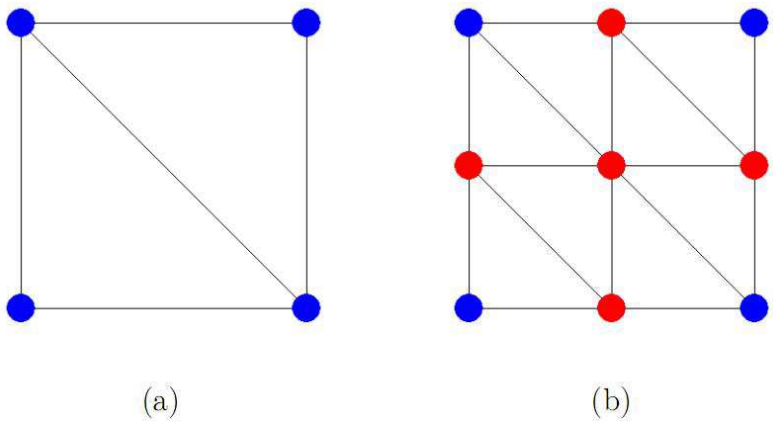

Figure 3.6: (a) The original data points shown in blue; (b) generated new points in red after recursive subdivision.

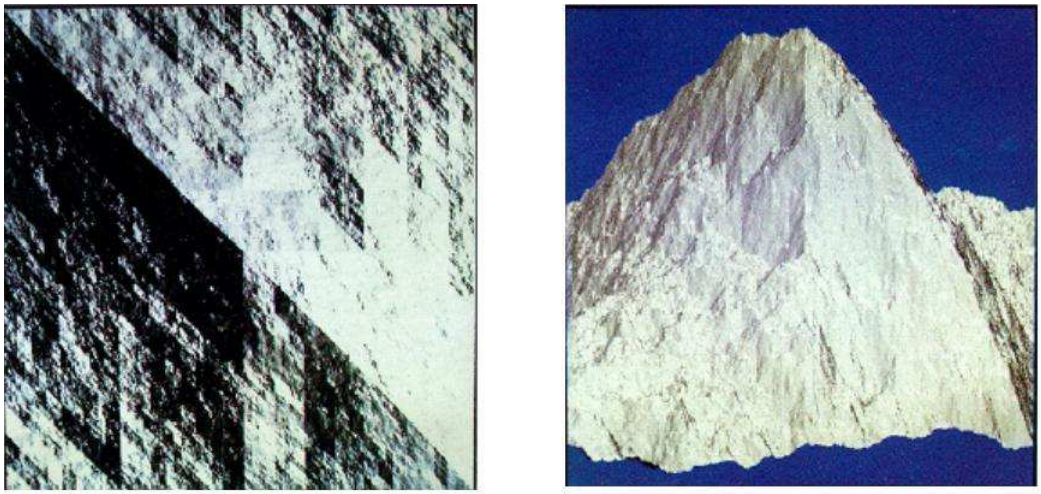

(a) (b)

Figure 3.7: (a) Top view of generated terrain; (b) side view of generated terrain.

Fig. 3.7 (a) and (b) are respectively top and side views of generated fractal terrain by using triangular-edge subdivision method. The problem for this method is some visual artifacts, such as creases. Creases are the parallel lines as can be seen quite clearly in Fig. 3.7 (a). They occur due to the no information pass between adjacent triangles. This is the deficiency of the method in generating fractal terrain [12, 19].

Diamond-Square Subdivision

In this algorithm, the midpoint is generated by averaging the four corners of the surrounding square or diamond. And a random offset value is added to the midpoint. Since subdivision does take values from neigbouring regions, it's context dependent. We can divide the algorithm into two steps as square and diamond step. It begins with a square 2D array and has a dimension $(2^n + 1)^2$. Initially, the four corners are set to a value and then the subdivision begins [12, 19].

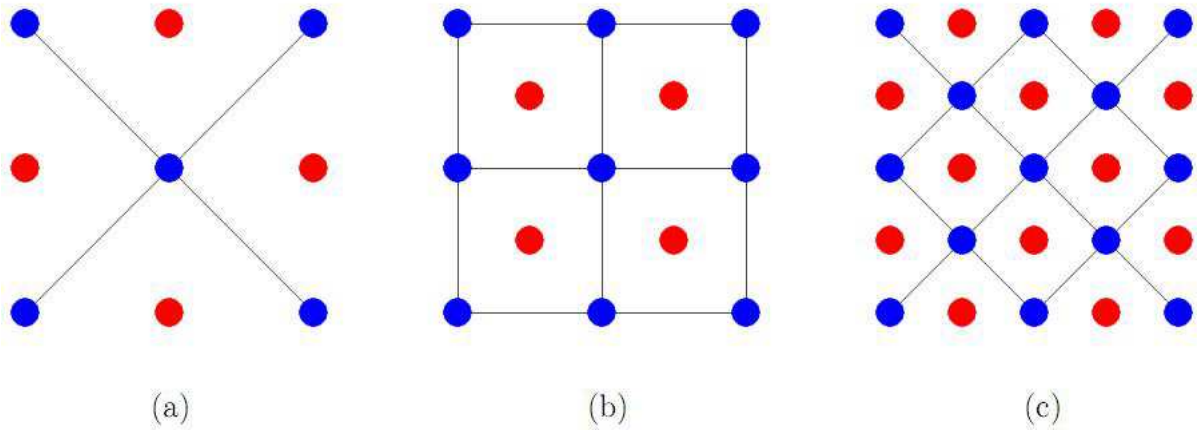

Figure 3.8: (a) The first diamond step showing half of each diamond; (b) the square step; (c) the next diamond step.

In square step, taking a square of four points, a value is generated at the square midpoint where the two diagonals meet. This midpoint value is calculated by averaging the four corner values, plus a random value. It gives us diamonds. In diamond step, taking each diamond of four points, a value is generated at the midpoint of the diamond again. This midpoint value is similarly calculated as the square step, by averaging the four corner points of diamonds, plus a random value. This step gives us squares. Subdivision continues until the all indices of the 2D array has set to a value [16, 17, 20]. These steps can be seen easily from Fig. 3.8. Fig. 3.8 a) is the first diamond iteration where the blue ones are the current data points and red ones are the newly generated points. Fig. 3.8 b) is the square step generating the red points. Fig. 3.8 c) is the next diamond step. The important point here is about the random value added in finding the newly generated midpoints of the squares and diamonds. These random values are selected from a range. If one square and diamond step can be thought as one iteration, then at the end of each iteration this random number range should be reduced by some factor. This random number range reducement is crucial in the roughness of the generated terrain. It specifies how jagged or smooth will be the terrain.

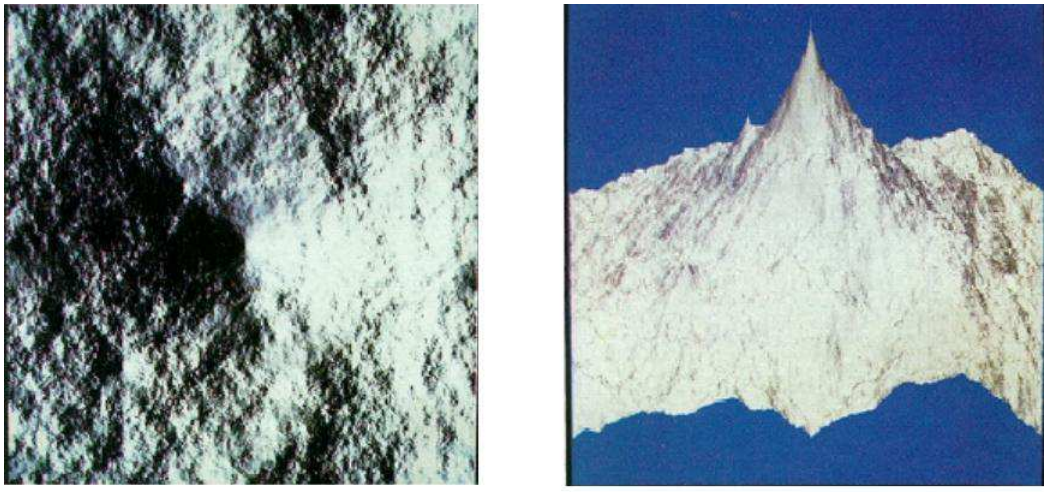

Figure 3.9: (a) Top view of generated terrain; (b) side view of generated terrain.

Fig. 3.9 (a) and (b) are respectively top and side views of generated fractal terrain by using diamond-square method. The problem of visual artifacts seen in triangular-edge subdivision such as creases, are not seen in diamond-square subdivision. It's due to the effect of neighbouring values in the generation of the midpoints of the diamonds and squares [12, 19].

Square-Square Subdivision

Square-square subdivion method is based on weighted averaging. As the name implies, division is realized by generating the new points on a square that is the half size of an existing square. This method is developed to eliminate the visual artifacts. It has some kind of interpolation in finding the new points of the square. Taken in the limit, these squares are getting smaller and naturally the points get arbitrarily closer which causes biquadratic surface. And this method will produce more smoother landscapes due to the interpolation [12, 19, 26].

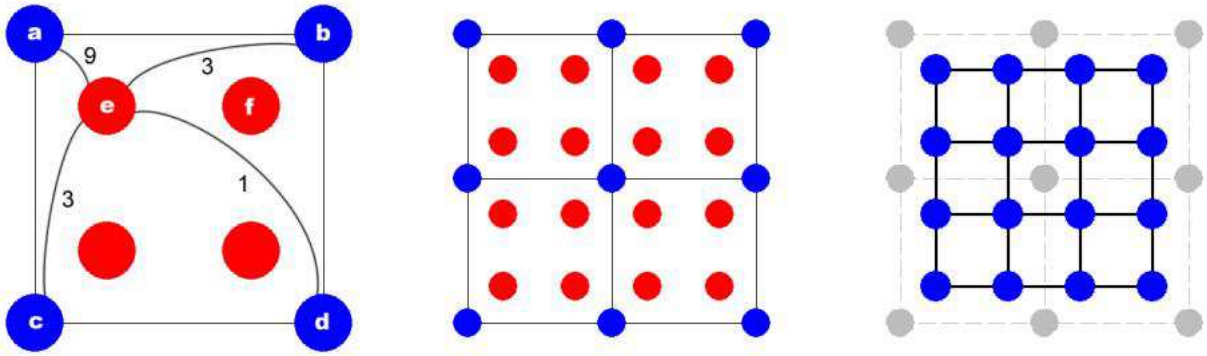

Figure 3.10: (a) Generating a new square vertices as weighted average of the surrounding vertices; (b) the first square iteration; (c) the second square iteration where the newly generated vertices become the new grid and the old grid is discarded.

Fig. 3.10 a) shows that the vertices of the new square are generated by a weighted average of the vertices of the original square. A random offset is also added to this amount.

$$e = \frac{9a + 3b + 3c + 1d}{16} + r, \tag{3.1}$$

$$f = \frac{3a + 9b + 1c + 3d}{16} + r, \tag{3.2}$$

where the r is the random offset, e and f is the new vertices of the new square and a, b, c, d are the vertices of old square shown as Fig. 3.10 a). The weighted average of the vertices is calculated as in Eq. (3.1) and Eq. (3.2). The vertice has more weight if it's near to the newly generated vertice. Fig. 3.10 b) and c) are respectively, the first and second iteration of the subdivision. The newly generated vertices become the new grid, whilst the old grid is simply discarded [19].

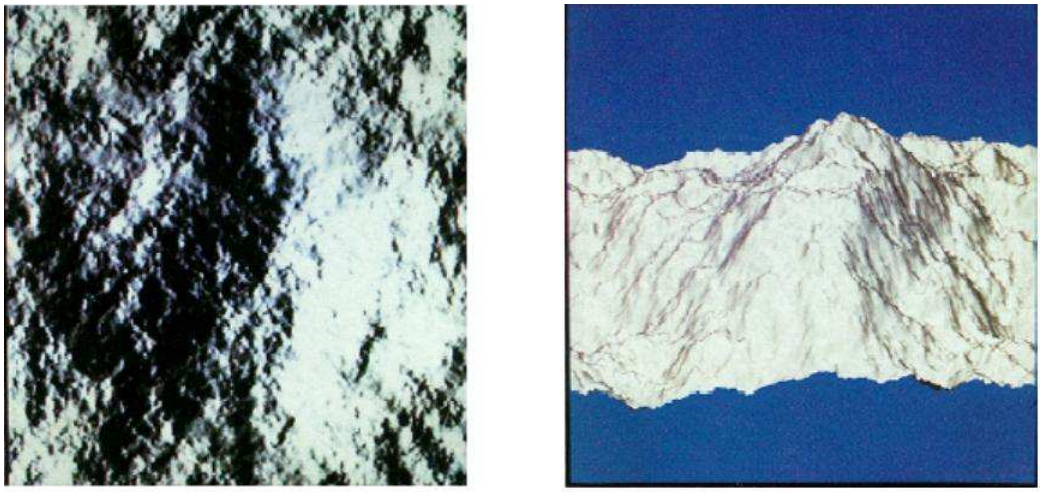

Figure 3.11: (a) Top view of generated terrain; (b) side view of generated terrain.

Fig. 3.11 (a) and (b) are respectively top and side views of generated fractal terrain by using square-square method. The visual artifact problem is minimized by means of the logic of the algorithm. And also, the generated terrain is very smooth [12, 19, 27].

3.2 Generated Fractal Terrain

After comparing many fractal techniques for generating a realistic synthetic terrain elevation data, we decided to use the diamond-square subdivision method for this purpose. In choosing this method, we have some considerations. First of all, the generated terrain has to be similar to a natural landscape as closely as possible. This means that visual artifacts, such as creases have to be reduced as much as possible. The roughness of the surface has to be close to the actual landscape. To sum up, all of these considerations with an easy implementation of the algorithm, the diamond-square method corresponds our requirements in generating a realistic fractal terrain. So, we decided to use this method.

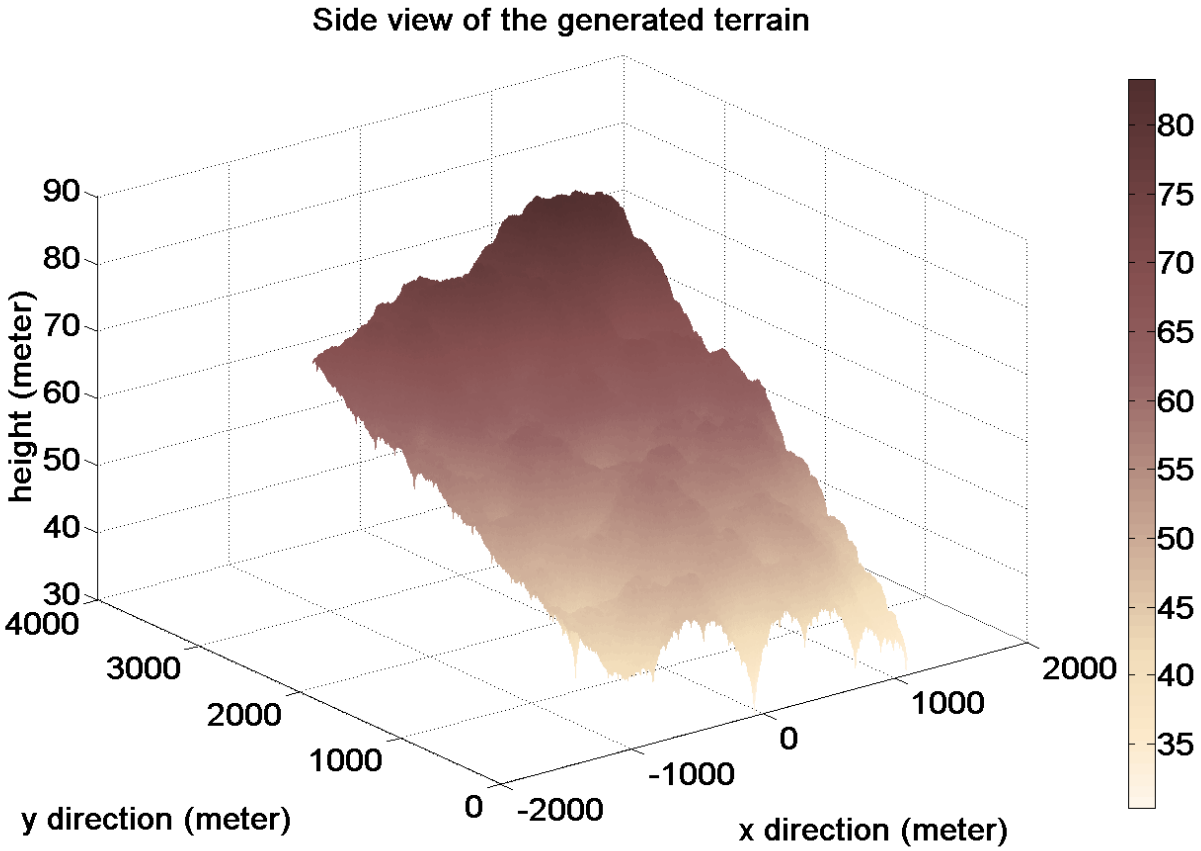

Figure 3.12: Three-dimensional side view of the generated fractal terrain.

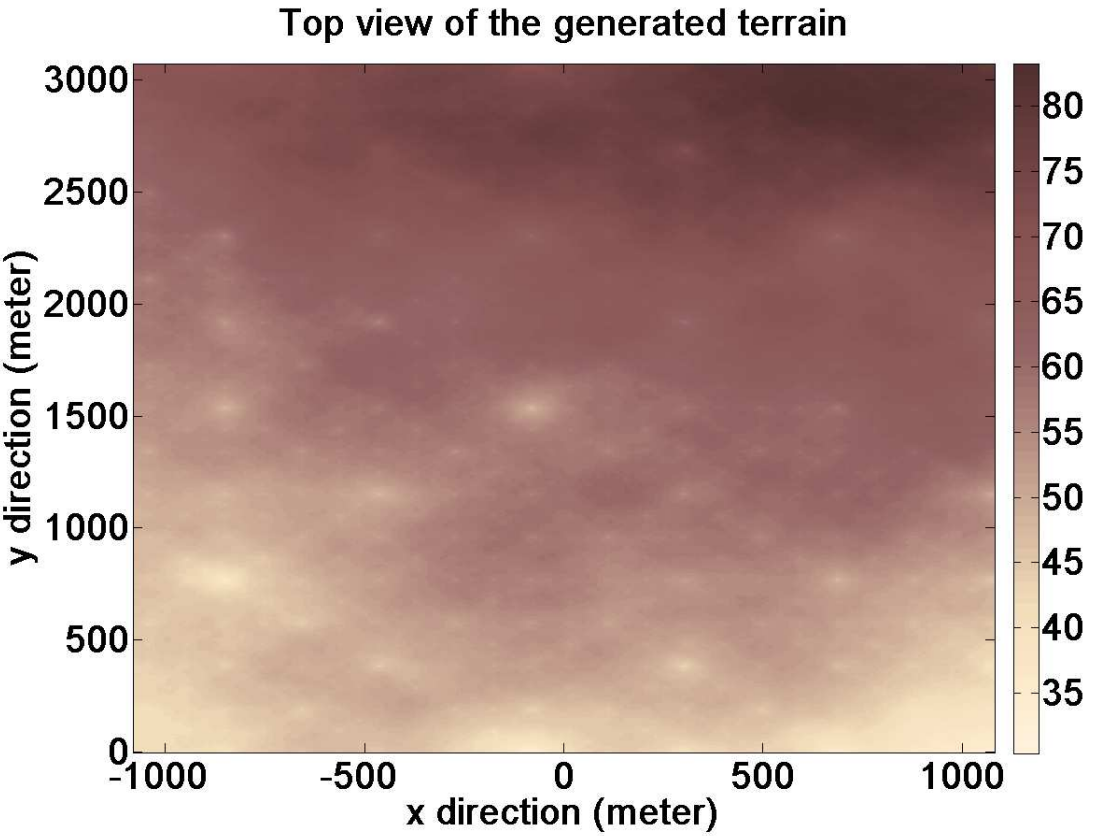

Figure 3.13: Top view of the generated fractal terrain.

Respectively, three-dimensional and top view of the sample generated synthetic terrain are shown with a (3,3) meter resolution in Fig. 3.12 and Fig. 3.13. Height changes between 30 and 90 meter for this sample synthetic terrain. As you can see, it's a very realistic landscape in overall aspect. The patches are small areas in the synthetic terrain. Fig. 3.14 shows the patches by zooming a region in the three-dimensional view. They are so realistic with their roughness as in the nature. Patches are important for the simulations. Because in each scan, each reflection is modelled as coming from a patch. The size of the patches are specified by the resolution.

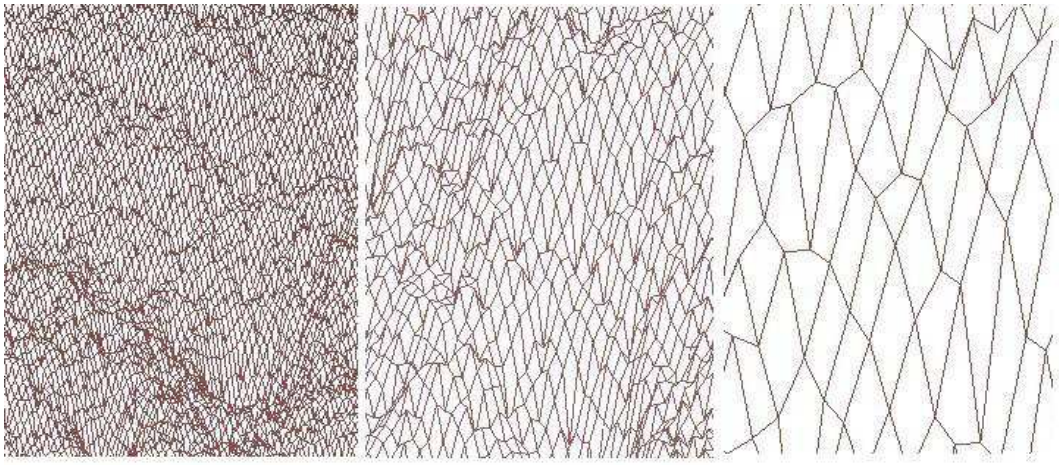

Figure 3.14: View of patches by zooming a region in the synthetic terrain.

3.3 Pulse-Doppler Processing

In simulation environment, a realistic synthetic terrain is generated. An aircraft can be simulated on this synthetically generated terrain by transmitting and receiving radar pulses. In the simulations, a pulse-Doppler radar is used for this purpose. In this section, a brief introduction is made to the transmitted signal shape and commonly used signal processing techniques on the received signals for the pulse-Doppler radars. This is mainly because of the fact that typical surveillance aircrafts carry pulse-Doppler radars, and here we investigate their usefulness for the terrain profiling.

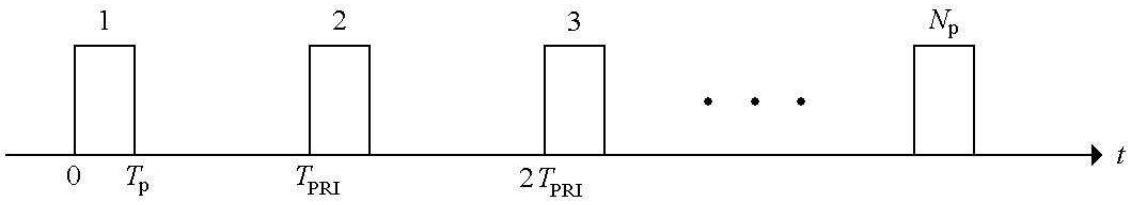

Figure 3.15: The signal structure used in the simulations.

Fig. 3.15 shows the signal structure that is used in the simulations. Here, N_p is the number of pulses that is transmitted by the antenna of pulse-Doppler radar. The time interval between the pulses is defined as "Pulse Repetition Interval" and symbolized as T_{PRI}. In the simulations, for every time duration of T_p, a pulse is transmitted and in the next duration of $T_{PRI} - T_p$, the receiver gets the echoes from the environment. So, the maximum and minimum distances of the echoes reflected from the synthetic terrain are calculated as in Eq. (3.3) and Eq. (3.4) [3, 28]. Here, c is the symbol for the light speed.

$$T_p = \frac{2R_{min}}{c}, \tag{3.3}$$

$$T_{PRI} - T_p = \frac{2R_{max}}{c}. \tag{3.4}$$

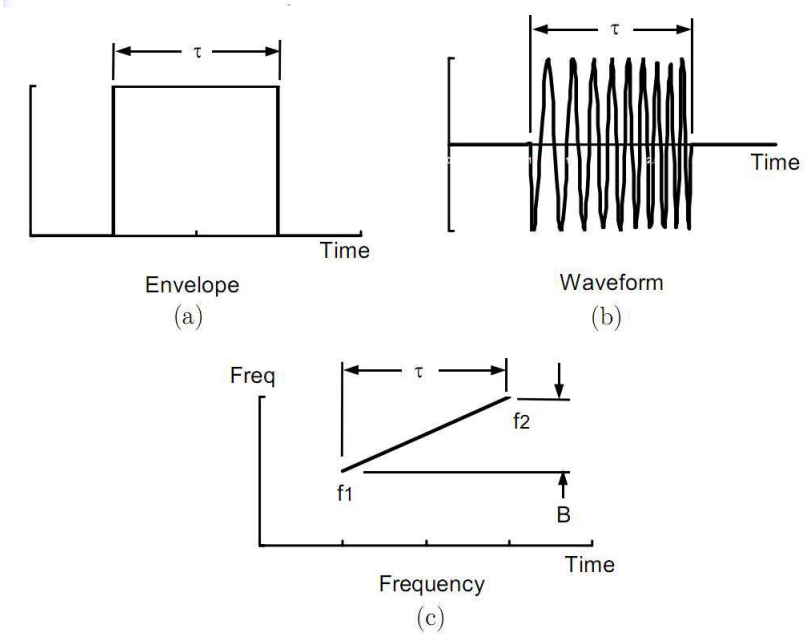

Figure 3.16: (a) LFM envelope sample; (b) LFM waveform sample; (c) LFM frequency sample.

The pulse shape in Fig. 3.15, is modulated by LFM (Linear Frequency Modulation) which is a commonly used modulation scheme in pulse-Doppler radars. LFM is also known as chirp modulation. Fig. 3.16 shows the LFM envelope, waveform and frequency sample. It has a constant envelope over time. In LFM modulation, frequency varies linearly with time over bandwidth B. For example, in Fig. 3.16, it has an increasing frequency. LFM have been heavily used in radar applications. For example, in demodulation of the received signals, matched filtering is used which will be discussed later. By means of LFM signal, the sidelobes of the matched filtered output of the received signal are decreased [3, 29].

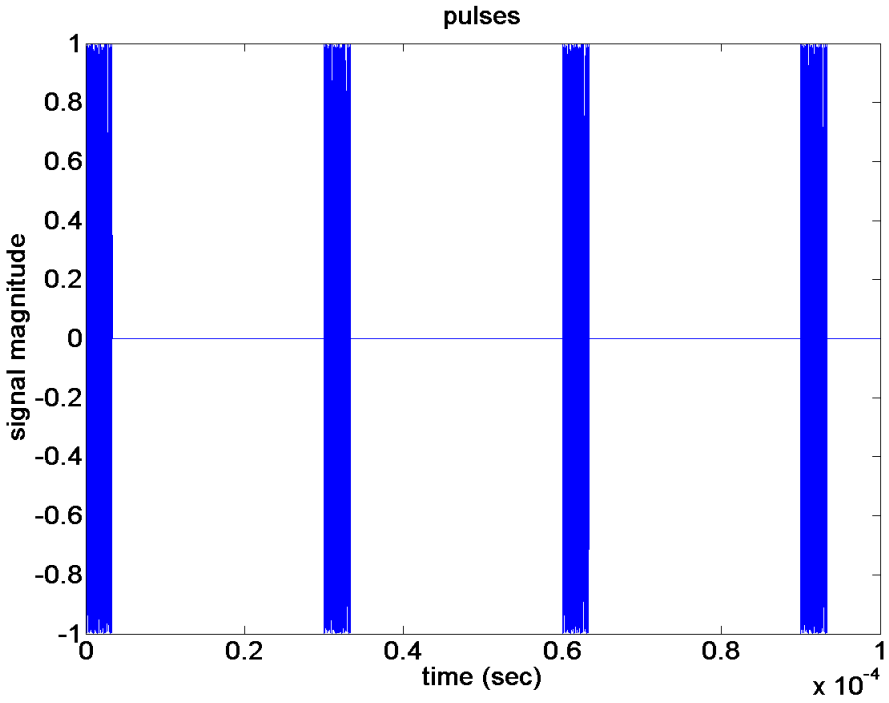

Figure 3.17: Generated pulse shape.

Fig. 3.17 shows a portion of the transmitted signal shape generated to be used in the simulations. This signal can be formulated as in Eq. (3.5).

$$x(t) = \sum_{i=0}^{N_p-1} a(t - iT_{PRI}) cos(2\pi(t - iT_{PRI})f_c + \frac{2\pi\beta(t-iT_{PRI})^2}{2T_p}), \qquad (3.5)$$

where N_p is the number of pulses transmitted, $a(t)$ is the pulse shape which is zero except $[0, T_p]$ interval, T_{PRI} is the pulse repetition interval, T_p is the pulse

duration, f_c is the carrier frequency and β is the bandwidth [3]. T_{PRI} and T_p values can be set to adjust the range interval of the reflections. In our simulations, reflections come between 500 and 4000 meter range values.

In pulse-Doppler radars, pulse-Doppler processing is applied on the received signals. Pulse-Doppler processing consists of pulse compression which is usually matched filtering, and FFT techniques. By means of this processing, the doppler shift-range plane is obtained. These are commonly used in radar signal processing [3]. Let $r(n)$ be the received signal for $n = 1, 2, ..., \frac{N_p(T_{PRI}-T_p)}{T_{samp}}$, where N_p be the number of pulses, T_{PRI} be the pulse repetition interval, T_p be the pulse length and T_{samp} be the sampling period of the analog signal. From that $r(n)$ signal, the R matrix is formed such that

$$R[i,j] = r[(i-1)\frac{T_{PRI}-T_p}{T_{samp}}+j], \quad i = 1, 2, ..., N_p, \;\; j = 1, 2, ..., \frac{(T_{PRI}-T_p)}{T_{samp}} \quad (3.6)$$

In Eq. (3.6), $R[i,j]$ shows the i^{th} row and the j^{th} column of the R matrix. Each row of the R matrix is matched filtered and pulse compression is realized.

Matched filtering is a commonly used technique on radar signal processing for the pulse compression. It's the optimal linear filter in demodulating the received signal for maximizing SNR (signal to noise ratio) in the presence of AWGN (a white gaussian noise). The impulse response of the matched filter is

$$H(f) = kS^*(f)exp(-j2\pi f t_d), \quad h(t) = ks^*(t_d - t), \quad (3.7)$$

where $s(t)$ is the input signal, k is a constant and t_d is a time value to make $h(t)$ casual. The choice of t_d does not effect SNR value [30].

So, for the LFM modulated pulses used in the simulations ,the matched filter is defined as

$$h(n) = p^*(-nT_{samp}), \quad n = 1, 2, ..., \frac{T_p}{T_{samp}}, \tag{3.8}$$

where $p^*(t)$ is the complex conjugate of the LFM pulse, T_p is the pulse duration and T_{samp} is the sampling period.

After matched filtering each row of the R matrix in Eq. (3.6), Y matrix is calculated as in Eq. (3.9).

$$Y[i, :] = R[i, :] * p^*(-nT_{samp}), \quad i = 1, 2, ..., N_p. \tag{3.9}$$

By taking the column-wise FFT of the Y matrix like in Eq. (3.10), an unambiguous function A matrix is obtained. It's the doppler shift-range plane which has the information about the radial speed and range of the clutter according to radar. In radar literature, clutter is named as the echoes returned from ground, sea, rain, animals etc [3].

$$A[:, j] = FFT(Y[:, j]), \quad j = 1, 2, ..., \frac{T_{PRI}}{T_{samp}} + 1. \tag{3.10}$$

So, by means of this pulse-Doppler processing on the received signals, it can be extracted the necessary information about the clutter from the doppler shift-range plane. These clutter information can be processed to estimate the terrain profile.

Lastly, the antenna pattern used in the simulations, have a sinc shape over the elevation and the azimuth directions. Antenna gain changes according to the sinc function from the center of the beam to the sides through the elevation and azimuth angles.

Chapter 4

TERRAIN PROFILE

In this chapter, the detailed description of the techniques used for estimating the terrain profile is mentioned. Simulations are run on the created simulation environment mentioned in chapter 3 for applying these techniques. We compare these techniques with their estimation performance, in obtaining the optimum error results. Fig. 4.2 shows the general structure of the simulations in a block diagram.

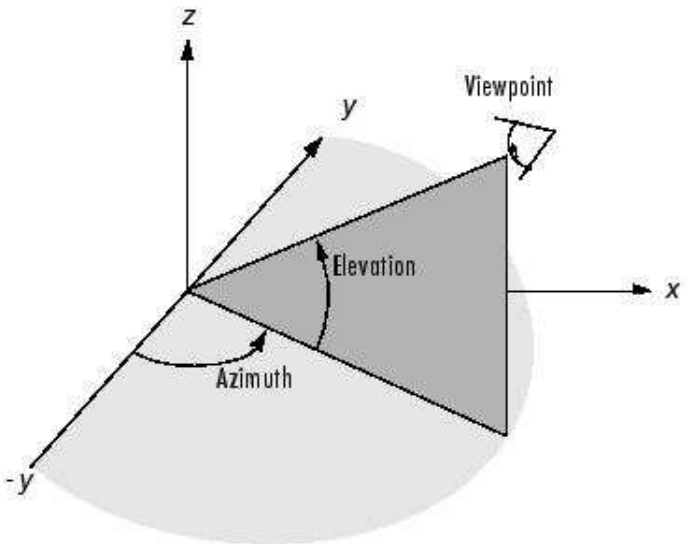

Figure 4.1: Azimuth and elevation angles.

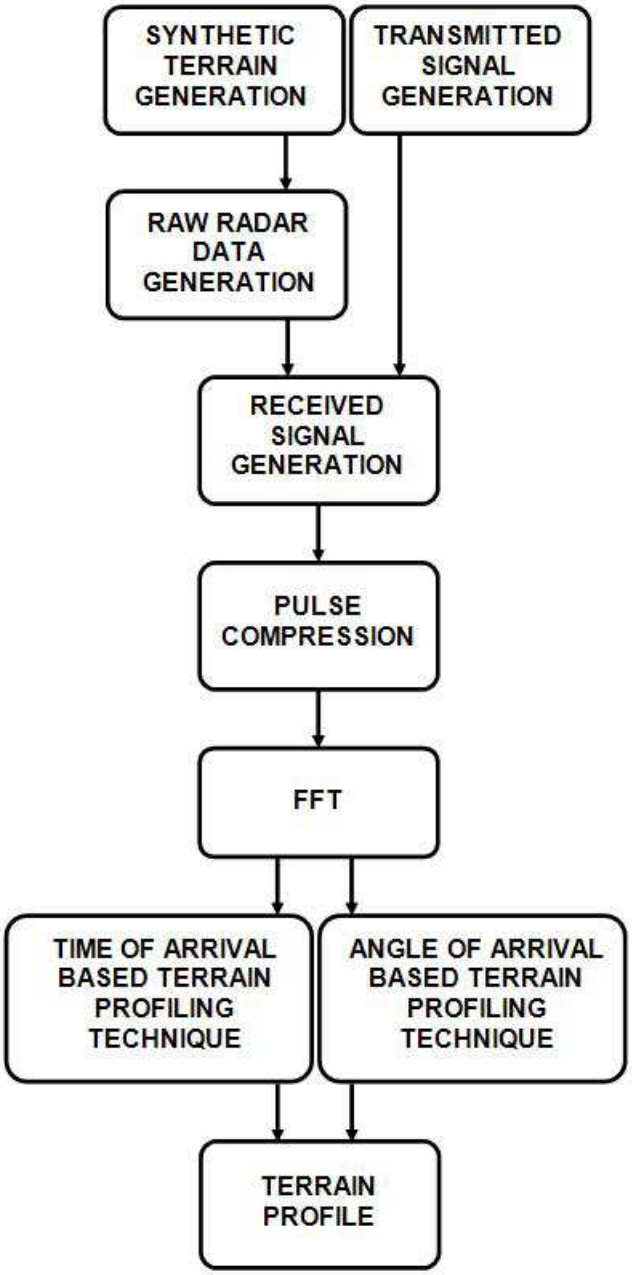

Figure 4.2: The general block diagram of the simulations.

Firstly, a synthetic terrain and the transmitted signal are generated in simulation environment to be used in the simulations. There is a pulse-Doppler radar antenna mounted on the aircraft. It scans the terrain by transmitting an LFM pulse train. Antenna has a beamwidth in azimuth and elevation angles. Azimuth and elevation angles are defined according the viewpoint of an eye, as

in Fig. 4.1. For each technique, there is a particular scanning pattern which will be discussed in detail during the techniques. Pulse-Doppler radar antenna beam illuminates the generated synthetic terrain according to the scanning pattern. There are reflections from the patches of the synthetically generated terrain where antenna beam illuminates. Raw radar data generation block produces the necessary raw radar data from these reflections to be used in the generation of the received signals. Received signal generation block uses these raw radar data and the transmitted signal for generating the received signals. These necessary raw radar radar data are respectively the distance, the area, the grazing angle, the azimuth and the elevation angle of the patch.

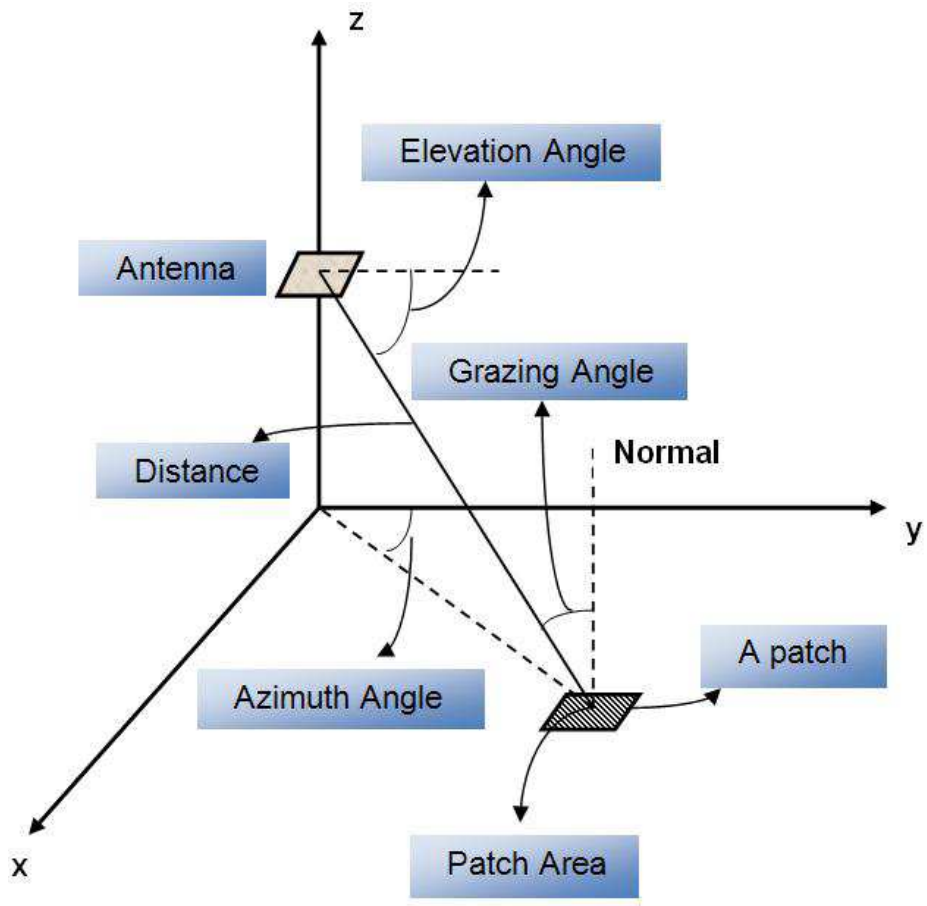

Figure 4.3: The illustration of the necessary raw radar data in axes .

Fig. 4.3 shows the schematic of the raw radar data collected between the antenna beam and a single patch. These raw data are used in generating the received signal as mentioned. Antenna transmits and receives the signal with an antenna pattern and gain. Antenna pattern used in the simulations, has a digital sinc shape which is periodic with 2π around the center of the beam through the azimuth and elevation angle. Received signal is another version of the transmitted signal that has some delay, energy and phase shift on it. The energy of the received signal is different than the energy of the transmitted signal. Antenna transmits the signal with different gain values according to the different azimuth and elevation angles using its pattern. RCS (radar cross section) is the measure of how detectable an object is with radar [3]. By using the RCS value of the patch, it can be found the certain amount of the energy reflected back from the patch. So, patch area and grazing angle are necessary to find the effective RCS value of the patch. There are phase shifts due to doppler effect and delay. We also need these raw radar data in finding these phase shifts. Elevation and azimuth angle is used in finding the doppler frequency, and distance is used in finding the delay time. We add random phase shift to the received signal to make the simulations more realistic. Briefly, received signal generation block uses the data generated by the raw radar data generation block and the transmitted signal for obtaining the received signal. Pulse compression and FFT block diagrams do the pulse-Doppler processing on the received signals as mentioned in chapter 3.3. As a result of this processing, the necessary clutter information can be obtained from the doppler shift-range plane, to be used in the estimation of the terrain elevation data. This clutter received signal information is processed by using time of arrival based terrain profiling technique and angle of arrival based terrain profiling technique to estimate the terrain profile.

4.1 Terrain Profile Estimation Technique Based on Time of Arrival Information

This is the first technique that is used in estimating the terrain profile. As the name implies, the time of arrival information of the signal is used in the estimation of the terrain profile. It's applied on the pulse-Doppler processed received signal as shown in Fig. 4.2. There is a particular scanning pattern of the simulations for each technique and the raw radar data has been generated according to this scanning pattern. Before going into details for time of arrival based terrain profiling technique, let's mention about the scanning pattern of this technique used in generating raw radar data.

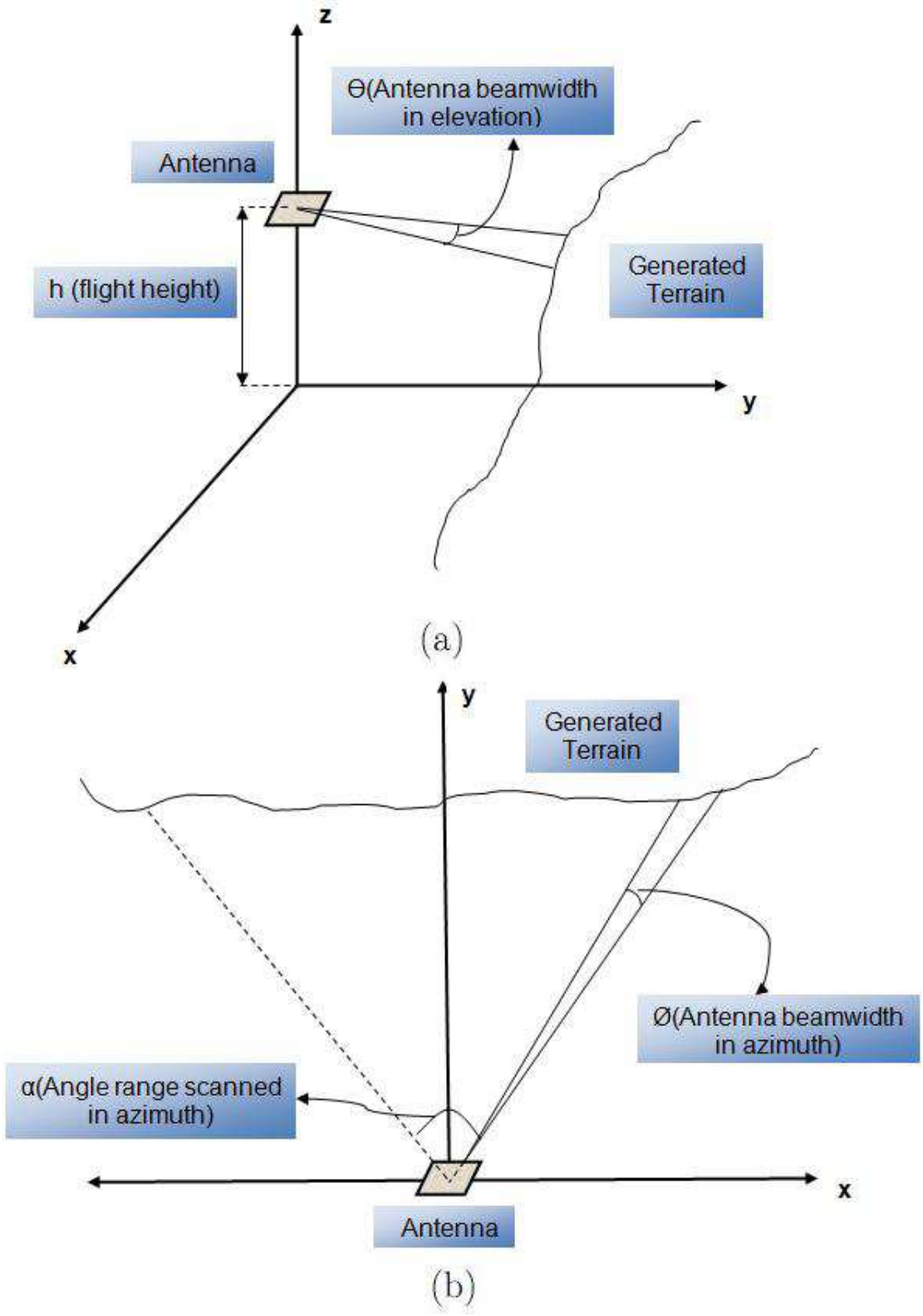

Figure 4.4: (a) The side view of the scanning pattern; (b) the top view of the scanning pattern.

Fig. 4.4 (a) and (b) show the pulse-Doppler radar antenna beams in the scanning pattern of the simulations made for time of arrival based terrain profiling technique. Accordingly, we have simulated aircraft flying straight, in 100 meter altitude, in y direction with constant 52 m/sec speed over the generated synthetic terrain. Radar antenna has a pencil beam in elevation and azimuth angles. These θ and ϕ angles which are the beamwidth of the antenna, are very small about 1 degree. With this pencil beam, aircraft scans the synthetic terrain in α degree angle range by turning the main antenna beam direction small amounts, like 2 degree, in each update. One scan is described as the complete scan of the α degree. For each update of the main antenna beam direction in one scan, the raw radar data is gathered to generate the received signal that is received from that corresponding angle. In these scans, antenna works as transceiver such that transmits and receives at the same time. The radar antenna transmits the generated signal form in Fig. 3.15 with N pulses in each update. The parameters of this signal form like T_p, T_{PRI} are adjusted to receive echoes between 500-4000 meter range. Briefly, this scanning pattern is used in raw radar data generation for time of arrival based terrain profiling technique.

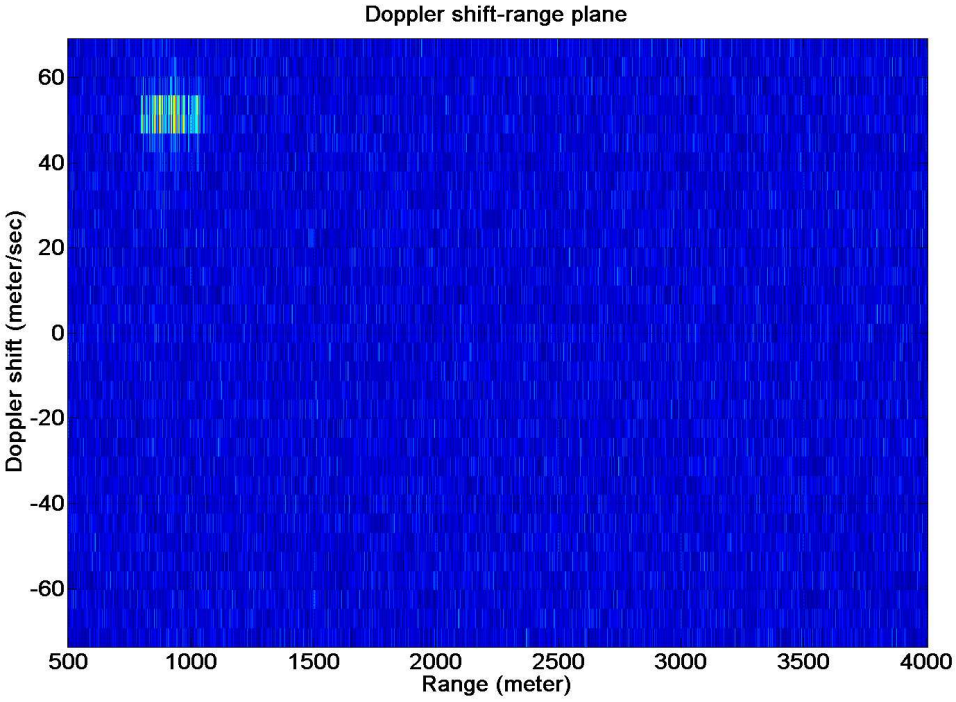

Figure 4.5: Doppler shift-range plane of a sample received signal.

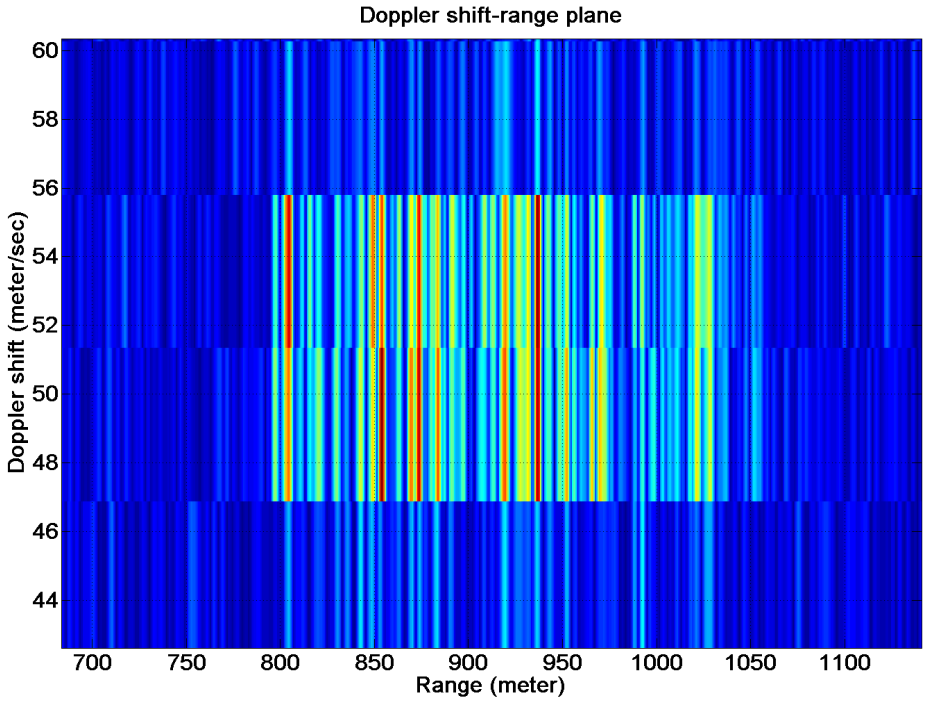

Figure 4.6: Zoomed view of the clutter in Fig. 4.5.

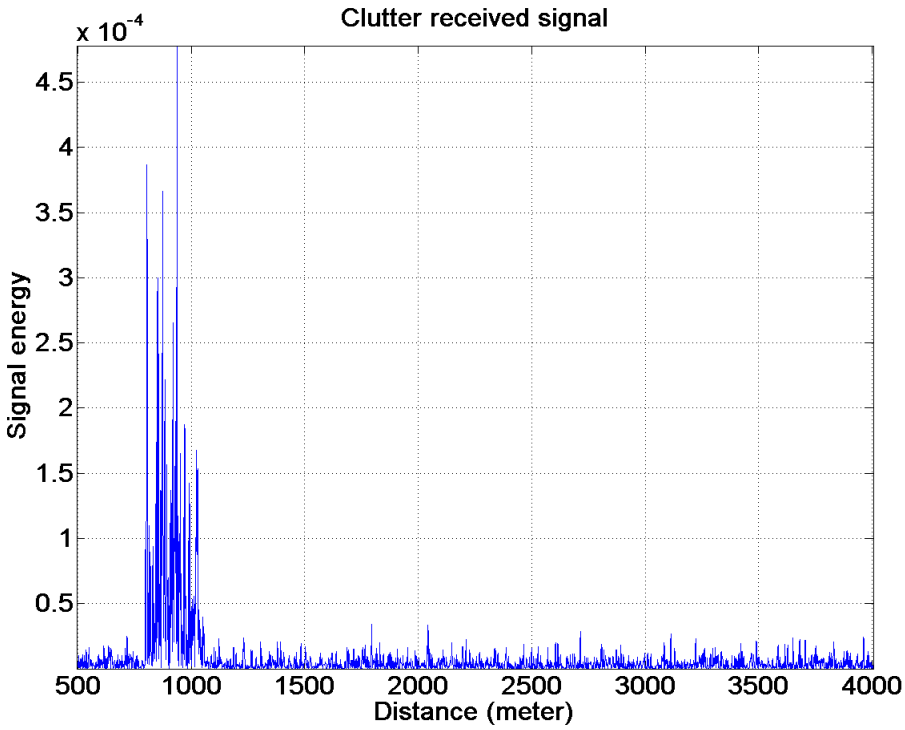

Figure 4.7: A sample clutter received signal.

In Fig. 4.5, the pulse-Doppler processed received signal sample can be seen in doppler shift-range plane. As it's mentioned before, received signals are generated for each angle update in a scan by using the corresponding generated raw radar data. By using pulse-Doppler processing on these received signals, the dopler shift-range plane can be obtained like in Fig. 4.5. This plane shows the location of the echoes with their doppler and range bins. These echoes in the simulations are clutter received signals that are reflected from the patches of the synthetic terrain. When it's zoomed to the clutter in this plane like in Fig. 4.6, the doppler and range values of the clutter can be easily seen. Doppler shift values of the clutter are around 52 m/sec as expected. Because, during the simulations, aircraft is simulated with a 52 m/sec constant speed and the synthetic terrain is moveless. Since the doppler shift of the echoes from the synthetic terrain according to the aircraft is related with the relative velocity and the elevation angle between them, this is an expected result. By using these doppler shift-range planes for

each received signals, the corresponding clutter received signals are obtained. We can see in Fig. 4.6 that the clutter received signals spreaded over the doppler bins around 52 m/sec. We have used the maximum clutter received signal in the corresponding doppler bin as the detection signal in the estimation of the terrain profile. Fig. 4.7 shows the the maximum clutter received signal taken from the corresponding doppler bin of the Fig. 4.6. These clutter received signals will be used to estimate the terrain profile and time of arrival based terrain profiling technique is about the processing of these signals in the estimation of the terrain profile.

4.1.1 Edge Detection With An Adaptive Thresholding

The clutter received signal in Fig. 4.7 consists of the noise and the signal part. The aim here is to detect the edges of the signal part with an adaptive thresholding by seperating it from the noise part. By means of this edge detection, the first and the middle reflection range points in the signal part can be found. These reflection range points will be used in estimating the terrain profile. These reflection ranges are related with the time of arrival of the echoes. That's why the technique is based on time of arrival information. Let's mention how an adaptive threshold value is selected to detect the edges. The energy of the noise part is rather smaller than the energy of the signal part as it can be seen from Fig. 4.7. In setting the threshold value firstly, the signal is seperated to the windows with specified length and the mean energies of the signals in these windows are calculated. The size of the windows is a parameter in the algorithm. Fig. 4.8 shows the window energies of the clutter received signal. The maximum window energy is highly probable in the signal part of the signal. So, the median value of the window energies is taken. Because the median window energy is highly probable in the noise part. This window in the noise part can be used in setting the threshold value for detecting the edges. For this purpose, the maximum energy

value is chosen from that window with median energy. The threshold value is set to a k multiple of this maximum energy value. Here, k is a constant parameter. Since the window with median energy is in the noise part, k multiple of the maximum value of energy in that window has highly probable larger magnitude than the noise magnitude. And it has also smaller magnitude than the energy values in the maximum energy window. So, this value which is set as threshold, can be used to detect the edges of the signal part. Here, the window size and k constant are parameters and we try to use the optimum values of these parameters where this detection algorithm works well.

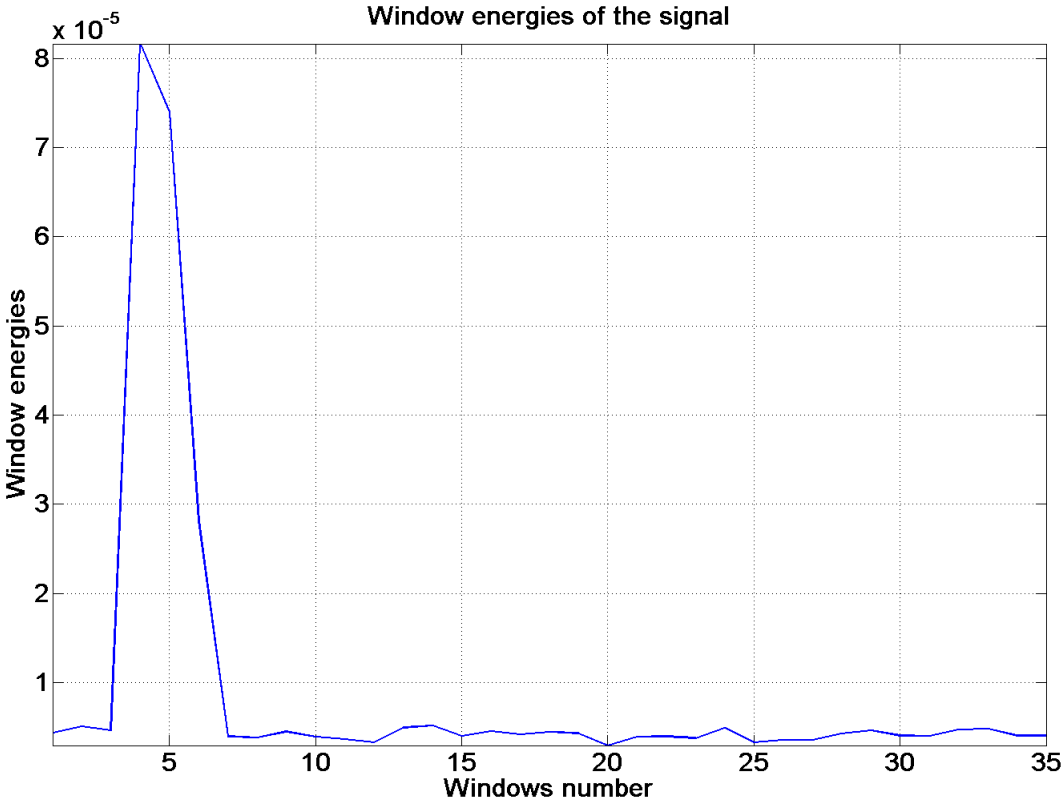

Figure 4.8: Window energies.

Fig. 4.9 is the figure of clutter received signal whose edges are detected with an adaptive threshold value. As it can be seen from the figure, the edges are detected with this adaptive thresholding method and the main part of the signal is shown

after this detection. The signal part is between 800 and 1050 meter range values approximately. This means that the echoes according to the aircraft position come from the range values between 800 and 1050 meter. Here, 800 meter is the first reflection range point and the middle reflection range point is the middle of the main signal part which is 925 meter here. These first and middle reflection ranges are found by means of this adaptive thresholding method. They will be used in estimating the terrain profile.

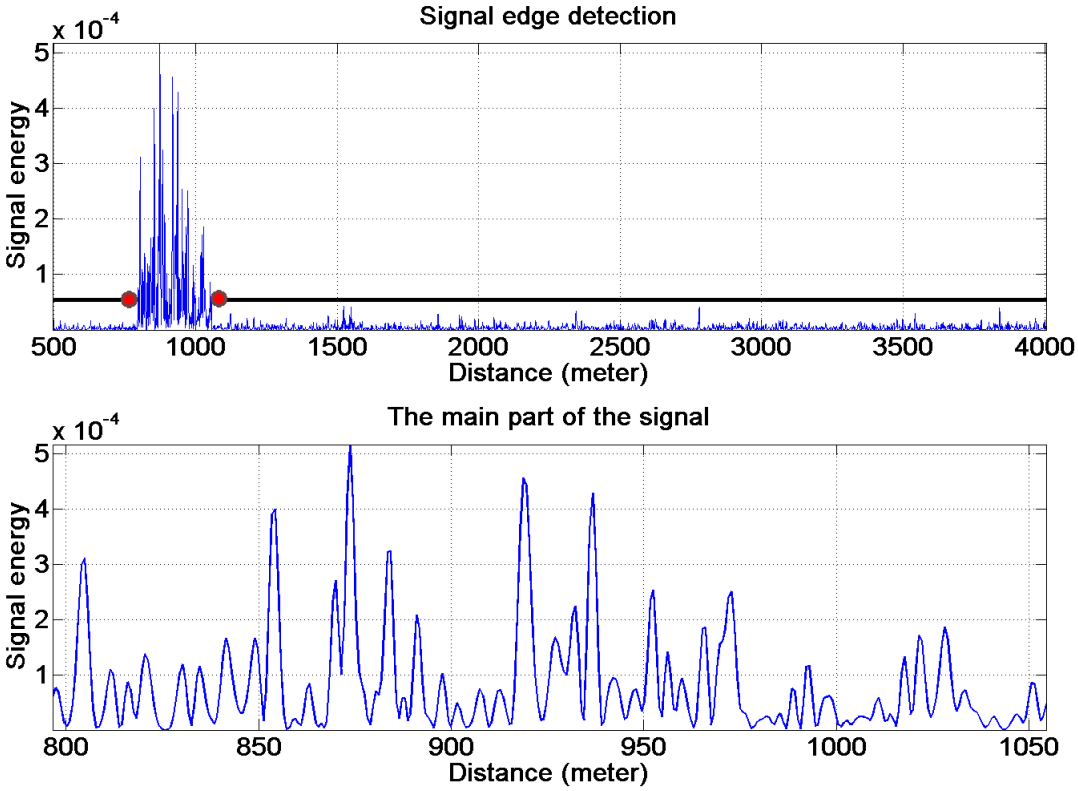

Figure 4.9: Edges detected clutter received signal and the detected part of that signal.

Rarely in this adaptive thresholding, there are some false detections due to the noise level exceeds the threshold value before the edges of the clutter received signal as shown in Fig. 4.10. Since this thresholding method is adaptive and it's realized with some parameters, these rare false detections occur. Although the

optimum parameter values are used, the algorithm can fail like this. But this problem in the algorithm is solved too. A correlation is observed between the detected range values of an angle in a scan and the detected range values of its neighbour angles in the same scan and consecutive scans. Fig. 4.11 is an example figure of the clutter received signal and its neighbour clutter received signals with some consecutive scans and consecutive angles. The observation is the existence of a correlation with the clutter received signal under test and the neighbour clutter received signals. We have focused on how much reliable this correlation value is. Therefore, we have looked at correlation coefficient values with consecutive scans and angles.

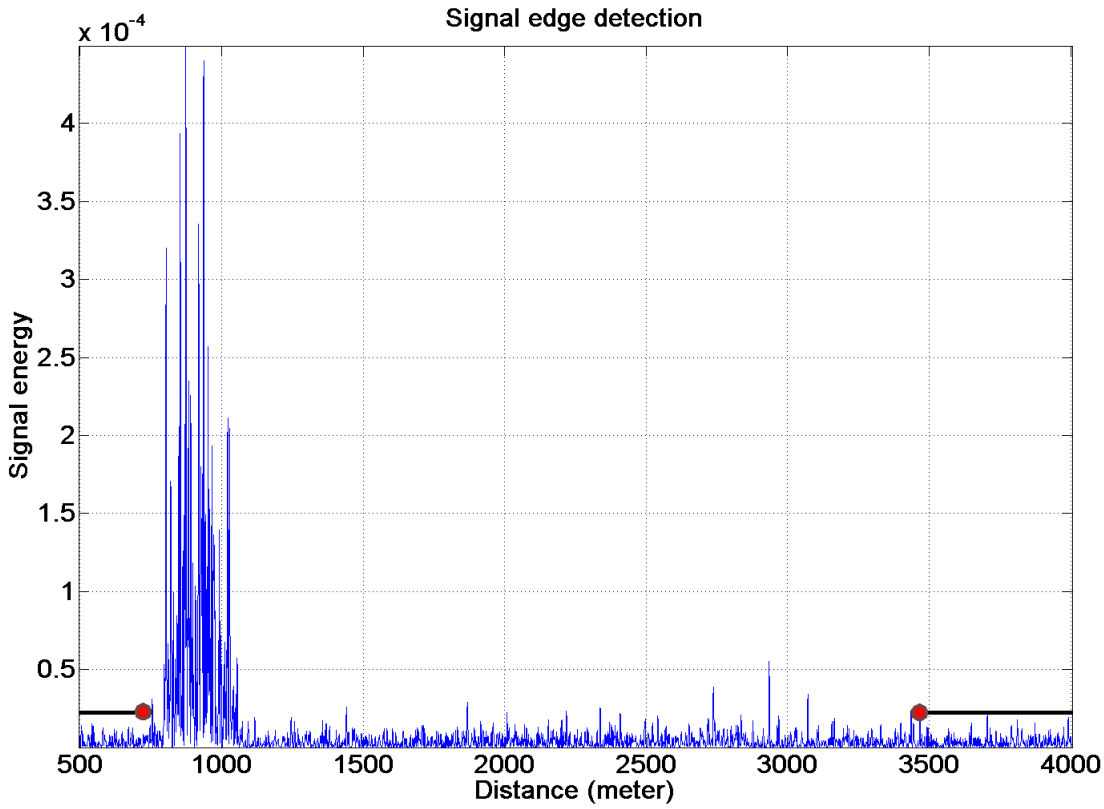

Figure 4.10: False detection with adaptive thresholding.

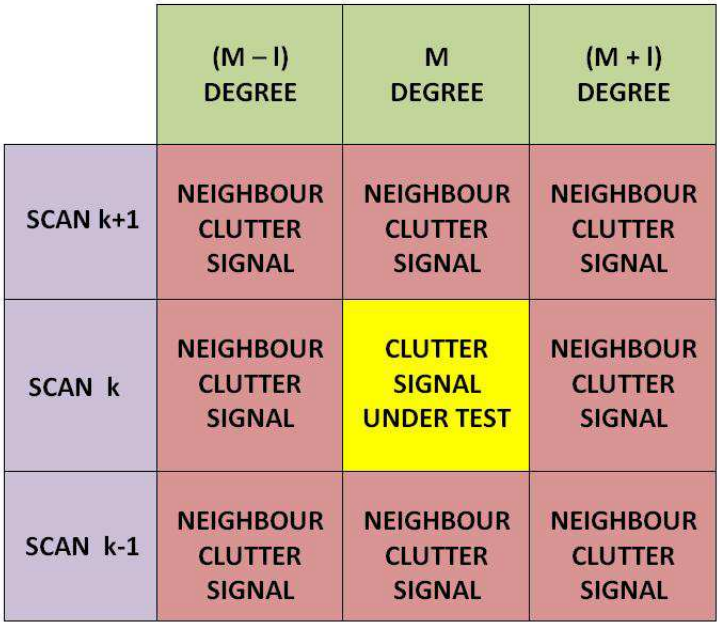

Figure 4.11: Clutter received signal in correlation with its neighbour clutter received signals.

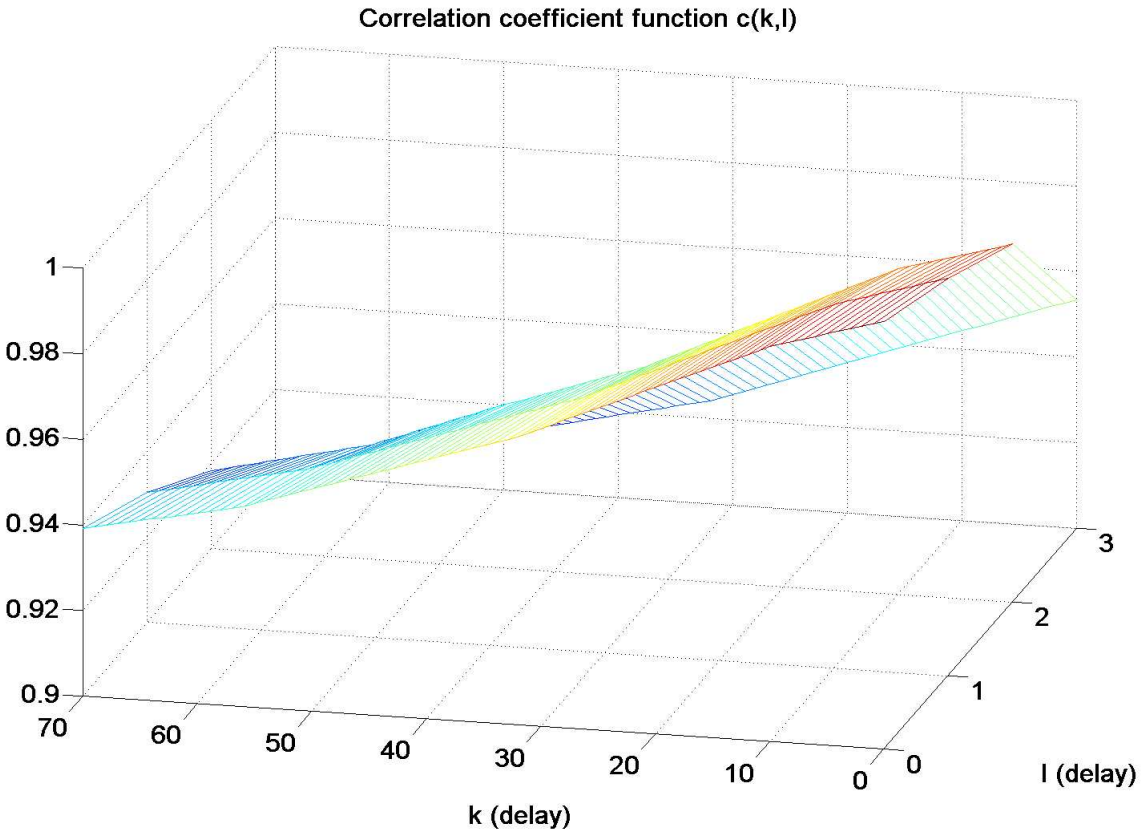

Figure 4.12: Correlation coefficient function between the first reflection range points of the clutter received signals.

$$r(k,l) = E(t(i_0, j_0)t(i_0 + k, j_0 + k)), \tag{4.1}$$

$$r(k,l) = \frac{1}{(2m+1)(2n+1)} \sum_{i=i_0-m}^{i_0+m} \sum_{j=j_0-n}^{j_0+n} t(i,j)t(i+k, j+l), \tag{4.2}$$

$$c(k,l) = \frac{r(k,l)}{r(0,0)}, \tag{4.3}$$

where k corresponds to consecutive scan number, and l corresponds to consecutive angle number.

Here in Fig. 4.12, the correlation coefficient function that is plotted according to the formulas Eq. (4.1), Eq. (4.2) and Eq. (4.3) is shown. The correlation coefficient between the first reflection range point of a clutter received signal under test and the first reflection range point of its neighbours in k and l axes, is very close to the maximum value 1. It means that there is a high correlation between them. So, this high correlation provides us a reliable information. If there is a false detection, it can be verified by comparing this false detected range of the clutter received signal with its correlated neighbour signal's first reflection range points. By means of this correlation, the rare false detections in adaptive thresholding can be checked and corrected.

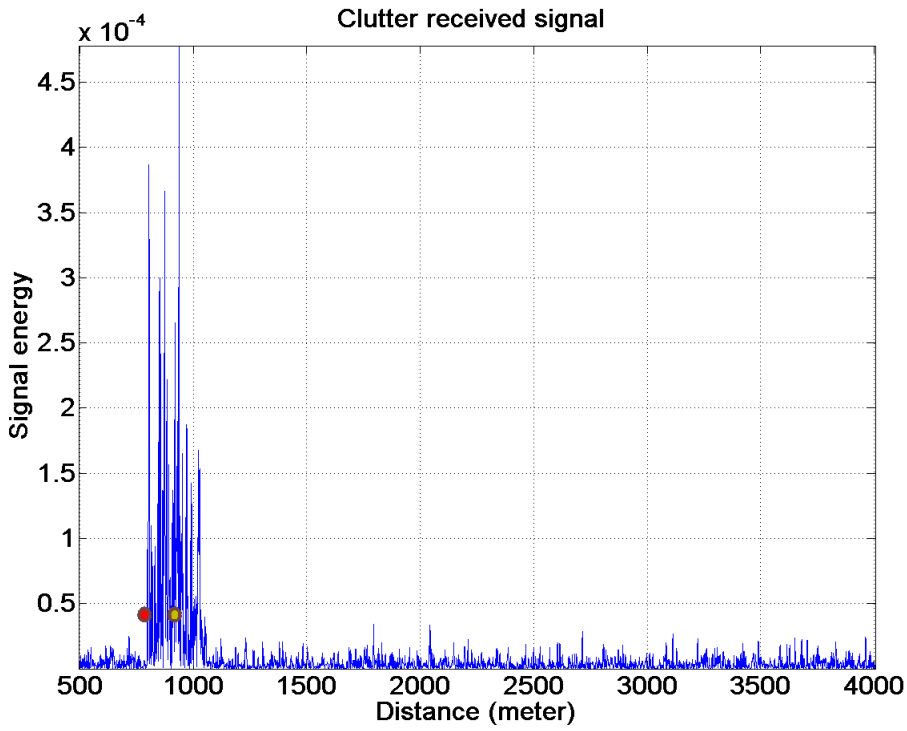

Figure 4.13: Clutter received signal with the first reflection range point (in red) and the middle reflection range point (in yellow).

This adaptive thresholding algorithm detected the edges of the clutter received signal successfully. The first and the middle reflection range points, shown in Fig. 4.13 with red and yellow marks, are used in estimating the terrain profile.

The first reflection range point is the first edge point and the middle reflection range point is the middle range point between two edges of the main part of the signal.

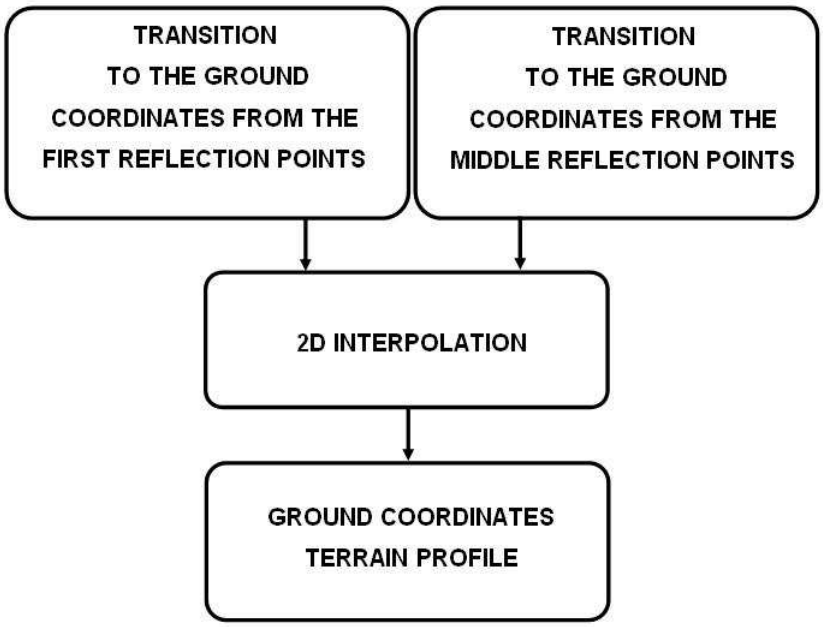

Figure 4.14: The general block diagram of time of arrival based terrain profiling technique.

Fig. 4.14 shows the general block diagram of time of arrival based terrain profiling technique in transition to the terrain elevation data from the first and the middle reflection range points. Since these range points are the ranges of the echoes from the synthetic terrain, we have used them to estimate the terrain profile. In transition to the ground coordinates from the first and the middle reflection range points, some geometrical calculations are used. Since the information like the flight altitude, the antenna beam direction with elevation and azimuth angle, the aircraft position, etc. are known during the simulations, it's easy to transit into the ground coordinates from the first and the middle reflection ranges with some easy geometrical calculations. What we've done is, putting height values to the corresponding x-y indices for each clutter received signal's first and middle reflection range points.

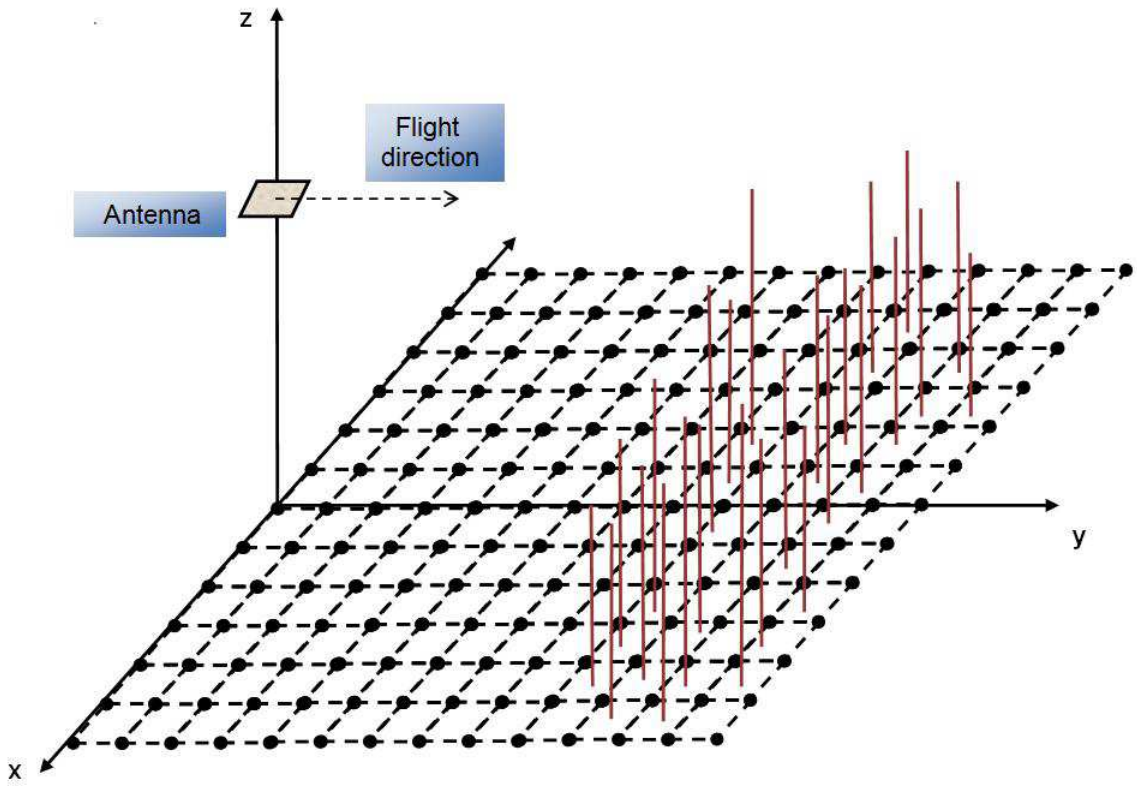

Figure 4.15: Transformation to the ground coordinates x-y-z by using the first and the middle reflection range points.

Fig. 4.15 is a sample illustration of the transformation to the ground coordinates x-y-z by using the first and the middle reflection range points. As aircraft flies straight along y direction, we put height values to the corresponding x-y indices for both the first and the middle reflection ranges. It includes simple geometrical calculation in transition from these range values to the ground coordinates. As it can be easily seen in Fig. 4.15, the height values seem like scattered sticks irregularly in the ground. The next step is, interpolating these irregularly scattered height values to the indices of a regular matrix. 2D interpolation is used to achieve this step.

$$g(k\Delta x, l\Delta y) = \sum_{i=1}^{N_d} W_{k,l,i} Z_i, \tag{4.4}$$

$$W_{k,l,i} = \frac{\frac{1}{d(x_i,y_i;k\Delta x,l\Delta y)}}{\sum_{m=1}^{N_d} \frac{1}{d(x_m,y_m;k\Delta x,l\Delta y)}}. \tag{4.5}$$

2D Interpolation of these scattered height values to a regular matrix is realized by Eq. (4.4) and Eq. (4.5). It basically weights the heights for finding height values of the regular matrix indices. In Eq. (4.4), g($k\Delta x$,$l\triangle y$) is the regular matrix with indice (k,l) and resolution (Δx,Δy) that is obtained from the 2D interpolation of the scattered height values. Here, Z is the scattered height values shown in Fig. 4.15. To find the height value of g($k\Delta x$,$l\triangle y$) indice, in a window of size N_d, every scattered Z_i value multiplied with a weight $W_{k,l,i}$ and these weighted Z_i values are summed. Here, the window size N_d is a parameter. Eq. (4.5) is the formula of finding every corresponding weight value $W_{k,l,i}$ for each Z_i value. $\frac{1}{d(x_i,y_i;k\Delta x,l\Delta y)}$ is the representation of the distance between the location (x_i,y_i) of Z_i height and the ($k\Delta x$,$l\Delta y$) indice of the regular matrix. It's obvious from the equation that the nearer Z_i's to the ($k\Delta x$,$l\Delta y$) indice of the regular matrix has larger weight values naturally. Consequently, with this 2D interpolation, the height values in a regular matrix in the ground coordinates are obtained. These height values in the regular matrix are namely the estimated terrain profile of the synthetic terrain. Let's have a look at what results we have obtained from the simulations by using time of arrival based terrain profiling technique.

4.1.2 Results

In this part, the results of the simulations by using time of arrival based terrain profiling technique are shown and investigated. The terrain profile is estimated for both the first and the middle reflection ranges. Their error performance is compared and the overall estimation performance is individually analyzed. The simulations are realized by an aircraft, flying straight along y direction, with

52 m/sec constant speed, in 100 meter constant altitude, over the synthetic generated terrain that has a (3,3) meter resolution. The scanning pattern has mentioned before.

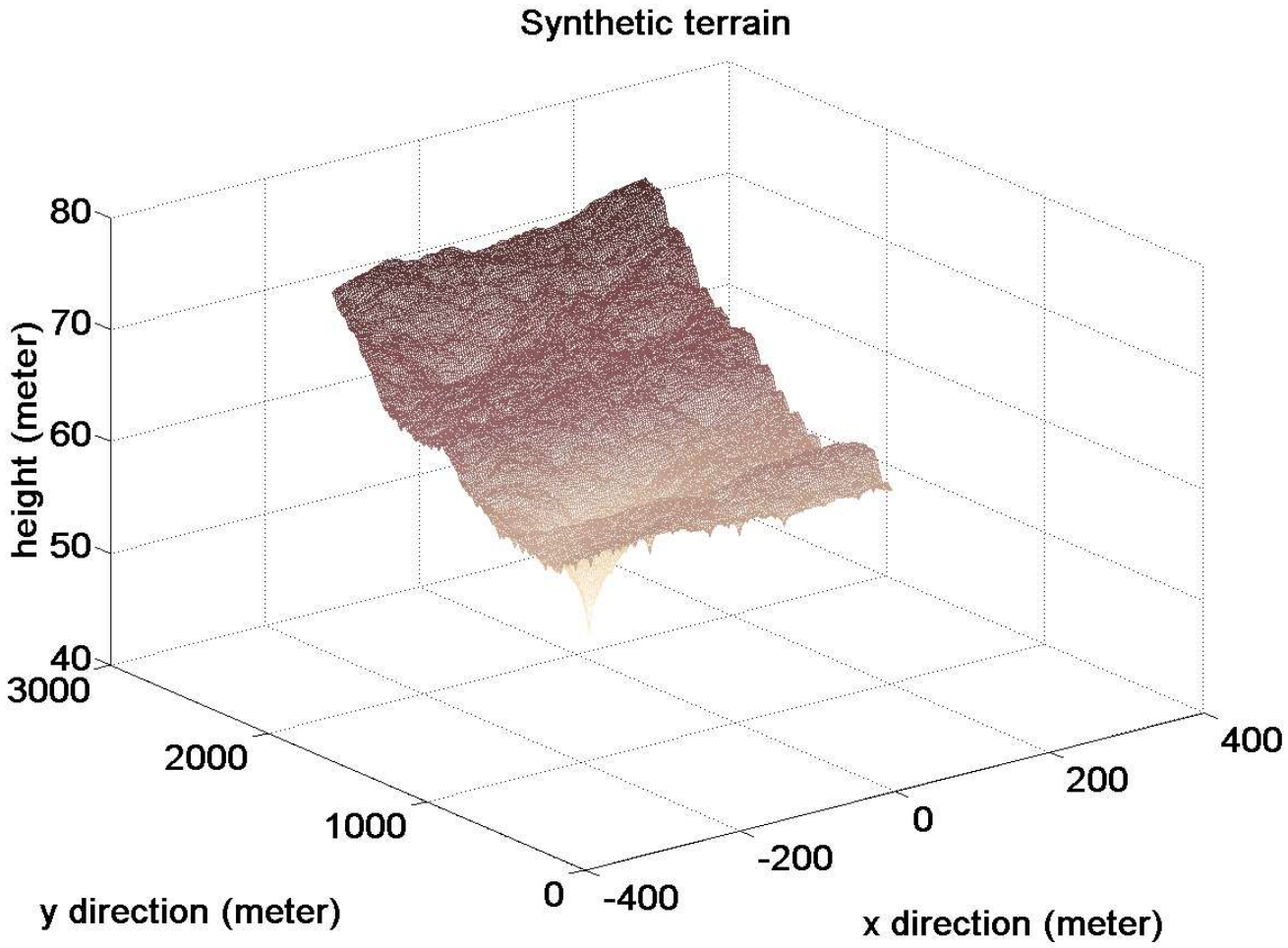

Figure 4.16: The side view of the synthetic terrain part, in the same location with the estimated terrain profile in Fig. 4.17.

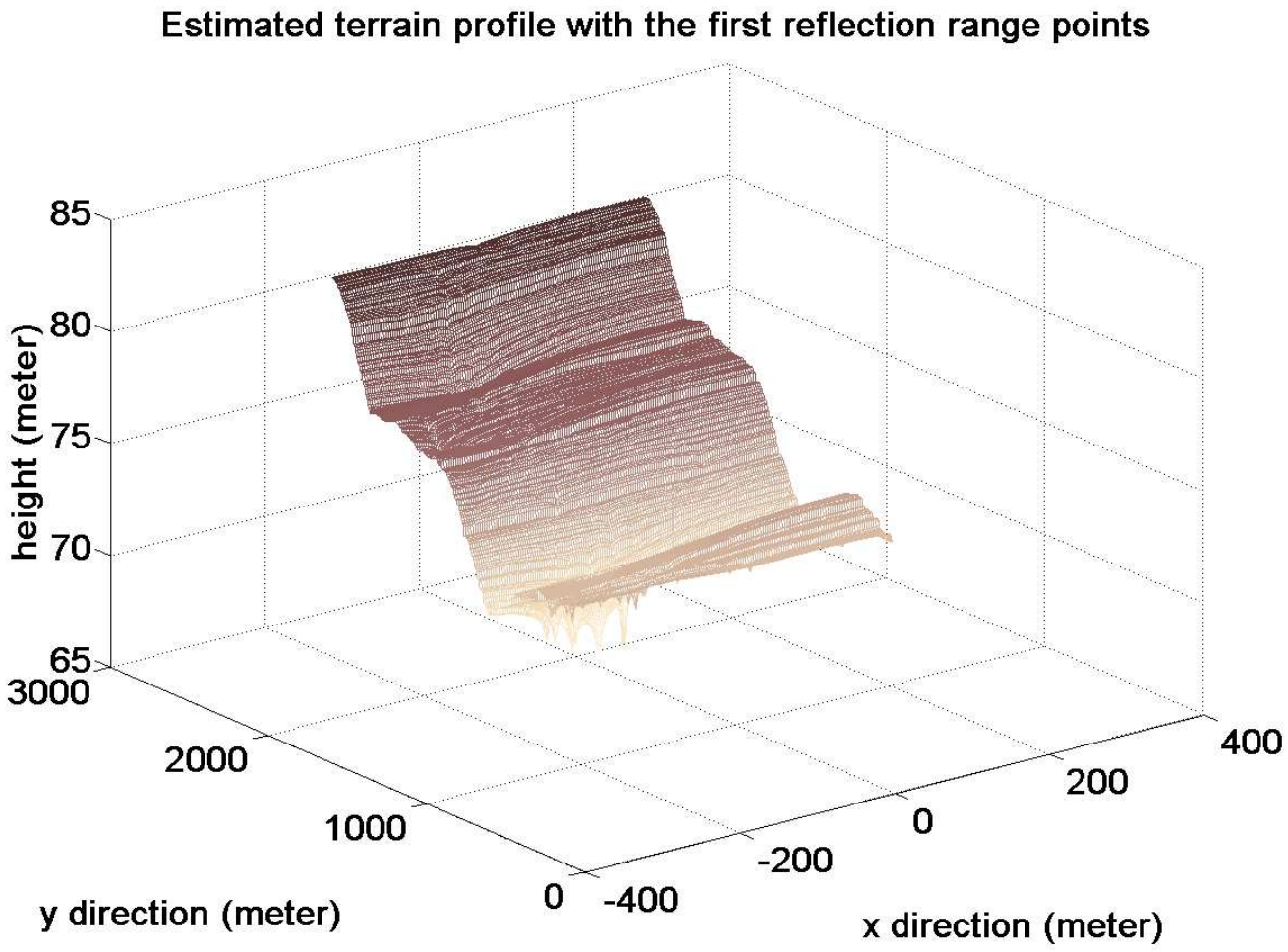

Figure 4.17: The side view of the estimated terrain profile obtained by using the first reflection range points.

Fig. 4.16 and Fig. 4.17 are respectively, the synthetic terrain and the estimated terrain results located in the same x-y location that is obtained with the usage of the first reflection range points. This is the result of many scans, obtained during the simulations by the aircraft flying straight along y direction, in 100 meter altitude, with 52 m/sec constant speed. In Fig. 4.17, the estimated terrain is figured only according to the results of all scans, not according to the last position of the aircraft. We can see that the general shape of the synthetic terrain in Fig. 4.16 is conserved in the estimated terrain profile with the usage of first reflection range points in Fig. 4.17. Using the first reflection range points

has a good performance in obtaining the general shape of the synthetic terrain. We have also looked at the error performance of that estimation which is more crucial.

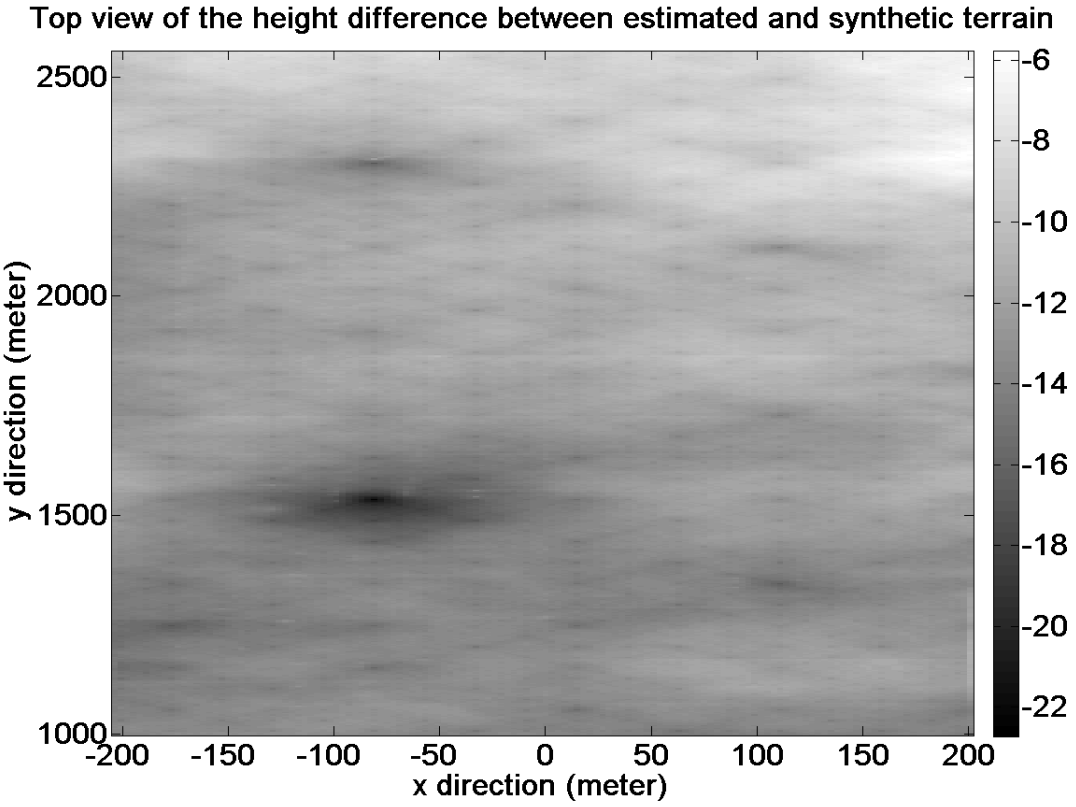

Figure 4.18: The top view of the height difference between the synthetic and the estimated terrain in Fig. 4.16 and Fig. 4.17.

Fig. 4.18 is the top view of the height difference between the synthetic and the estimated terrain for analyzing the error performance of that estimation with the first reflection range points. The mean error of the height difference is found as 12 meter and the maximum error of the height difference is found as 22 meter, for the simulations in 100 meter flying altitude. As you can see from the figure, around (-70m, 1500m) region, there is a hole in the shape of the synthetic terrain. Since in the simulations the antenna beam can not illuminate all of the depth of the hole, the maximum error occurs here. But it's not so important. The mean error performance is more crucial. We can say that the estimated terrain

from the first reflection range points has a successful estimation performance in conserving the general shape of the synthetic terrain and in the mean error value according to the flight altitude. We have also looked the performance of the middle reflection range points in estimating the terrain profile.

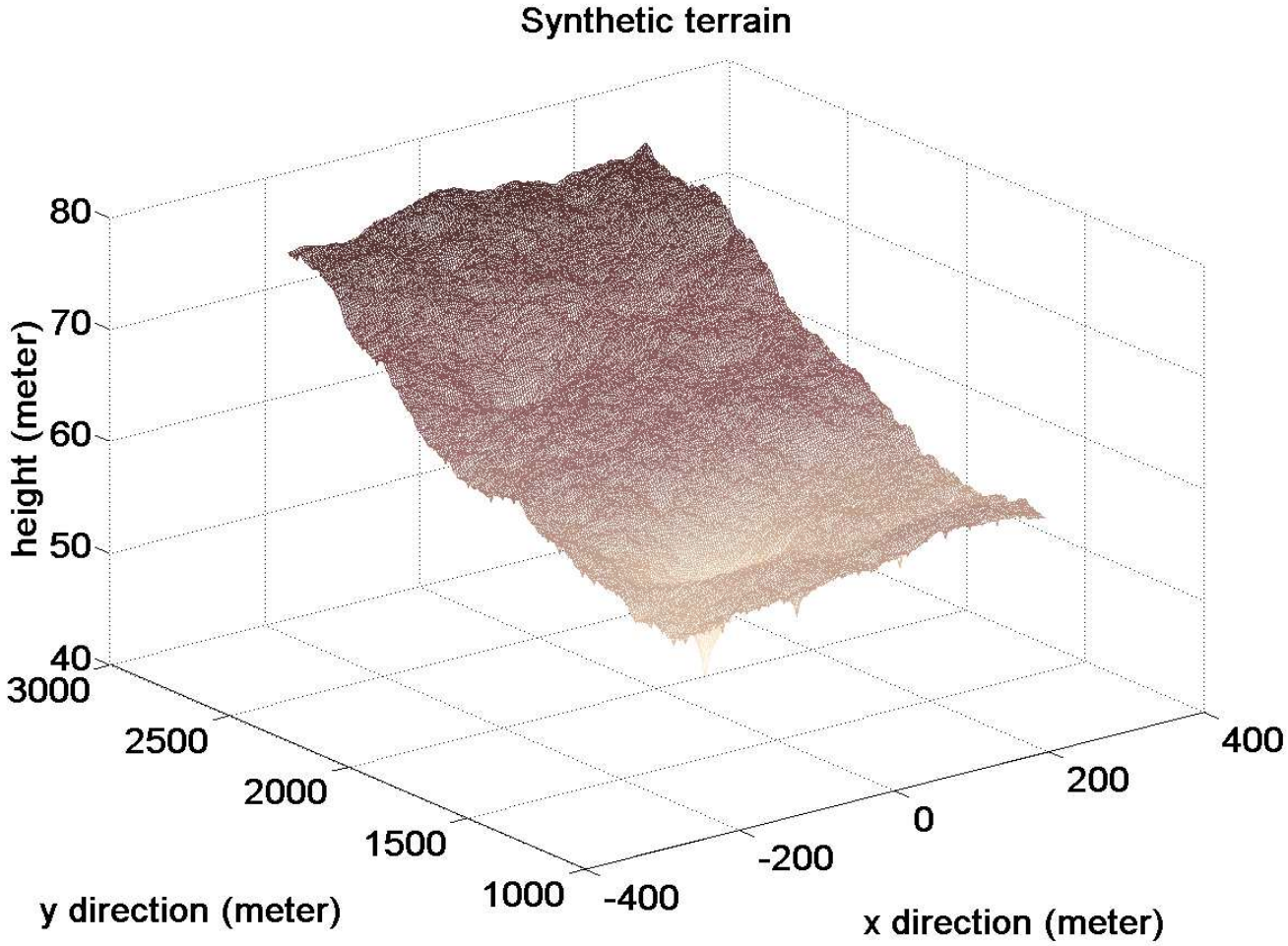

Figure 4.19: The side view of the synthetic terrain part, in the same location with the estimated terrain profile in Fig. 4.20.

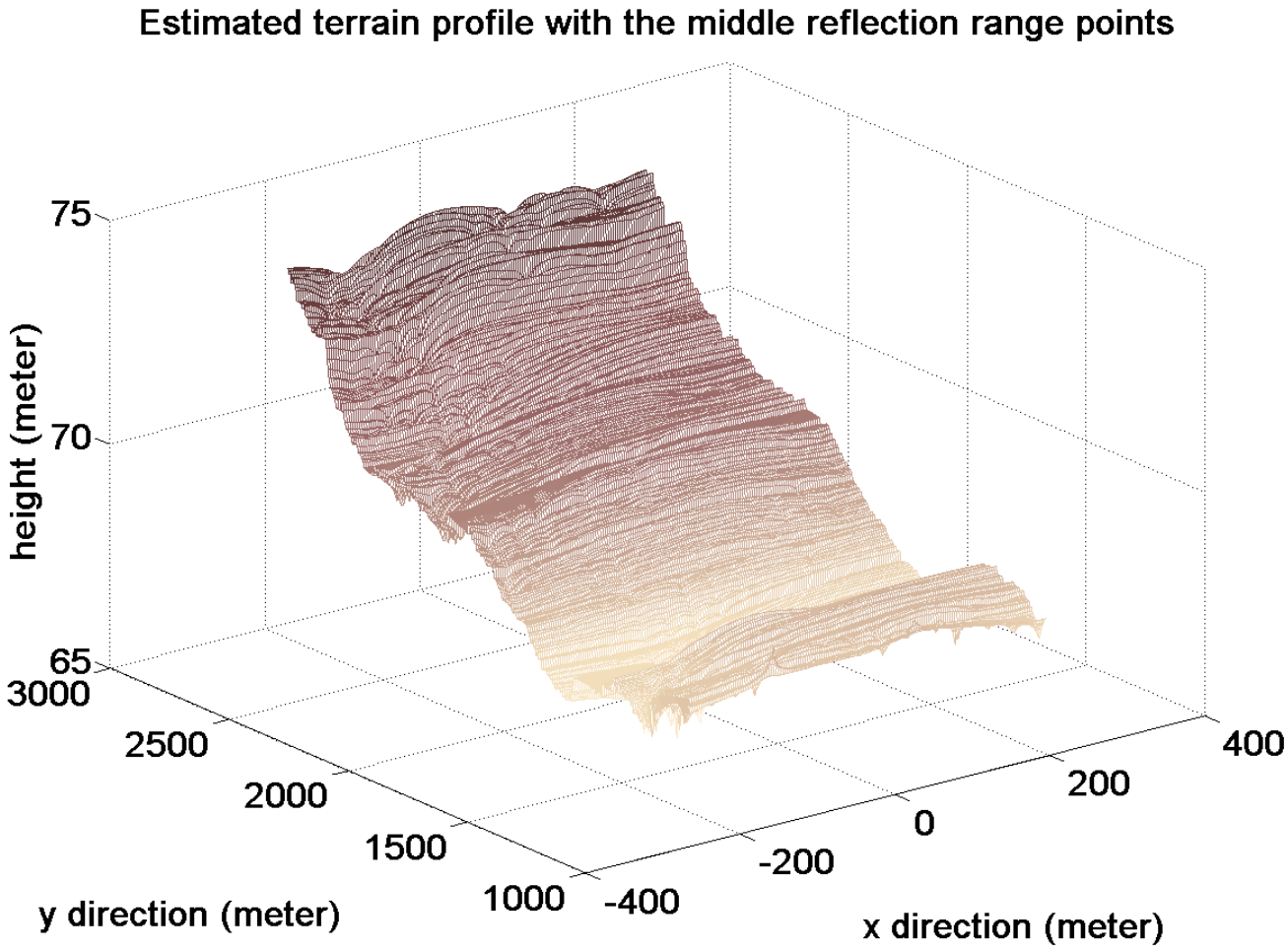

Figure 4.20: The side view of the estimated terrain profile obtained by using the middle reflection range points.

Fig. 4.19 and Fig. 4.20 are respectively, the synthetic terrain and the estimated terrain results located in the same x-y location, obtained with the usage of the middle reflection range points. Similarly, this is the result of many scans obtained by the aircraft flying straight along y direction, in 100 meter altitude, with 52 m/sec constant speed and the estimated terrain in Fig. 4.20 is figured only according to the result of the all scans, not according to the last position of the aircraft. The general shape of the synthetic terrain in Fig. 4.19 is conserved again successfully, in estimated terrain profile with the middle reflection range points in Fig. 4.20. But it has an improvement in the error performance of

the estimation of the middle reflection range points usage according to the first reflection points usage.

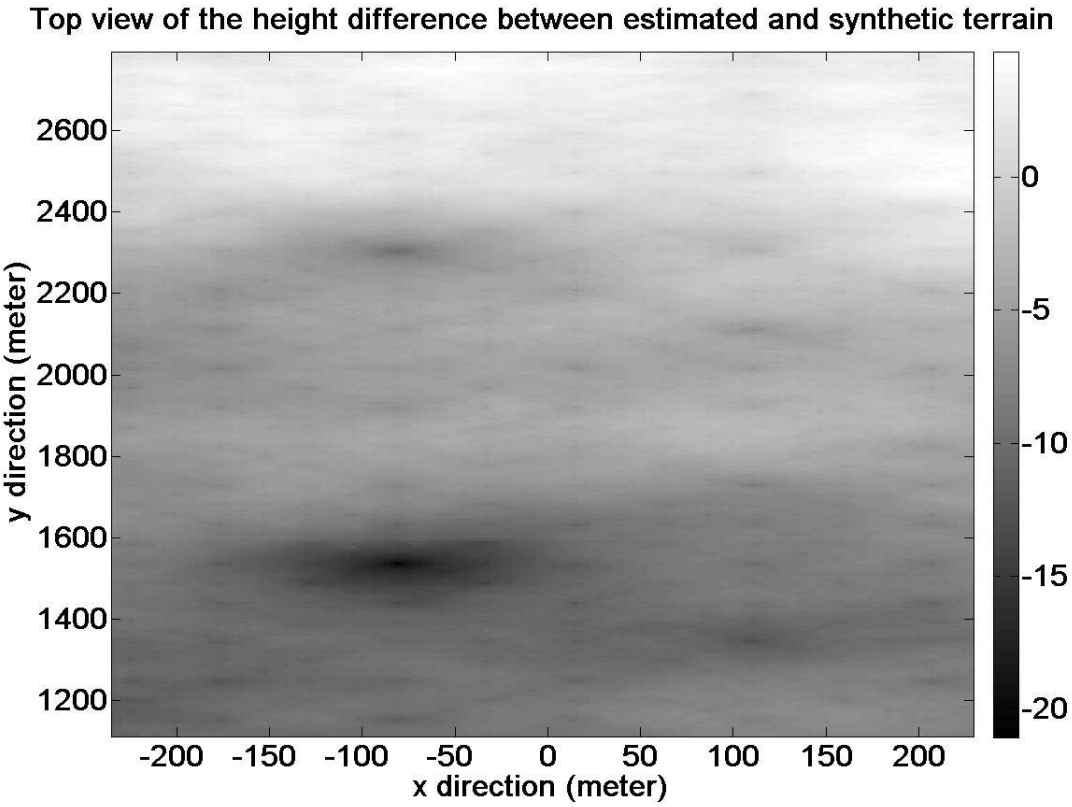

Figure 4.21: The top view of the height difference between the synthetic and the estimated terrain in Fig. 4.19 and Fig. 4.20.

Fig. 4.21 is the top view of the height difference between the synthetic and the estimated terrain for analyzing the error performance of the estimation with the middle reflection range points. This time, the mean error of the height difference is found as 6 meter and the maximum error of the height difference is found as 21 meter for the simulations in 100 meter flying altitude. The same reason with the previous result of the first reflection range points, the maximum error occurs around (-70m, 1500m) hole region. But the mean error performance of the middle reflection range points usage has obvious improvement according to the first reflection range points usage. The mean error of the middle reflection

range points usage decreased to 6 meter from 12 meter which is the mean error of the first reflection range points usage. We can conclude that both usage of the first and the middle reflection range points in time of arrival based terrain profiling technique has a good performance in estimating the terrain profile with similar shape and small error results. But the middle reflection range points usage has better performance in mean error values. We can explain this mean error improvement in the middle reflection range points usage. The antenna has illuminated an area of the synthetic terrain and echoes come back from that area. We have used the antenna's middle beam point's elevation and azimuth angle in transition to the ground coordinates, since we can't know the exact elevation and the azimuth angles of the echoes. The echoe that has come from the area of the antenna's middle beam point illumination is more probably in the middle reflection range of the clutter received signal rather than the first reflection range. That's why the middle reflection range points usage has better mean error performance in the estimation. Thus, time of arrival based terrain profiling technique is successfully fulfilled and let's have a look at the angle of arrival based terrain profiling technique.

4.2 Terrain Profile Estimation Technique Based on Angle of Arrival Information

Angle of arrival based terrain profiling technique is the other technique that is used in estimating the terrain elevation data. Similarly, it's applied on the pulse-Doppler processed received signal as shown in Fig. 4.2. It has a particular scanning pattern too, that the raw radar data has been generated accordingly. Before going into details for angle of arrival based terrain profiling technique, let's mention about the scanning pattern that is used in generating raw radar data. In this technique's simulations different from time of arrival based terrain

profiling technique, the antenna does not behave like a transceiver antenna. The transmitter antenna and receiver antennas are seperate. Fig. 4.22 (a) and (b) shows the transmitter antenna beams in the scanning pattern of the simulations made for angle of arrival based terrain profiling technique. Accordingly, we have simulated aircraft flying straight in 170 meter altitude, along y direction, with constant 52 m/sec speed. This time, the beamwidth of transmitter antenna θ and ϕ angles are different. θ angle in elevation is around 10 degree. On the other hand, ϕ angle in azimuth is very small around 1 degree. Aircraft scans the synthetic terrain by turning the transmitter antenna beam direction small amounts like in Fig. 4.22 (b), and in each update, the raw radar data is gathered to generate the received signal that is received from that angle. Samely, N pulses are transmitted in the generated signal form like in Fig. 3.15. Briefly, this scanning pattern is used in raw radar data generation for angle of arrival based terrain profiling technique.

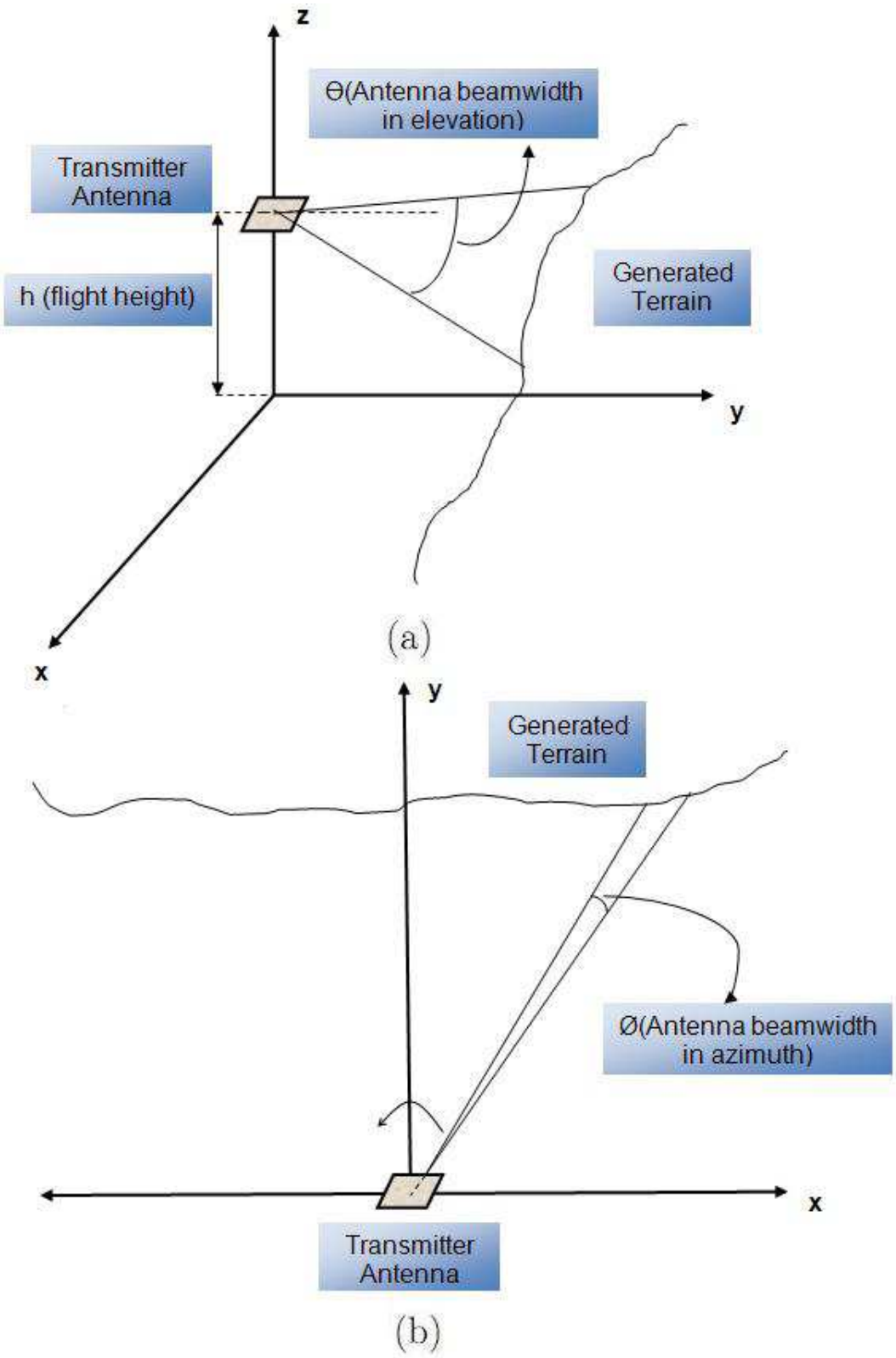

Figure 4.22: (a) The side view of the scanning pattern; (b) the top view of the scanning pattern.

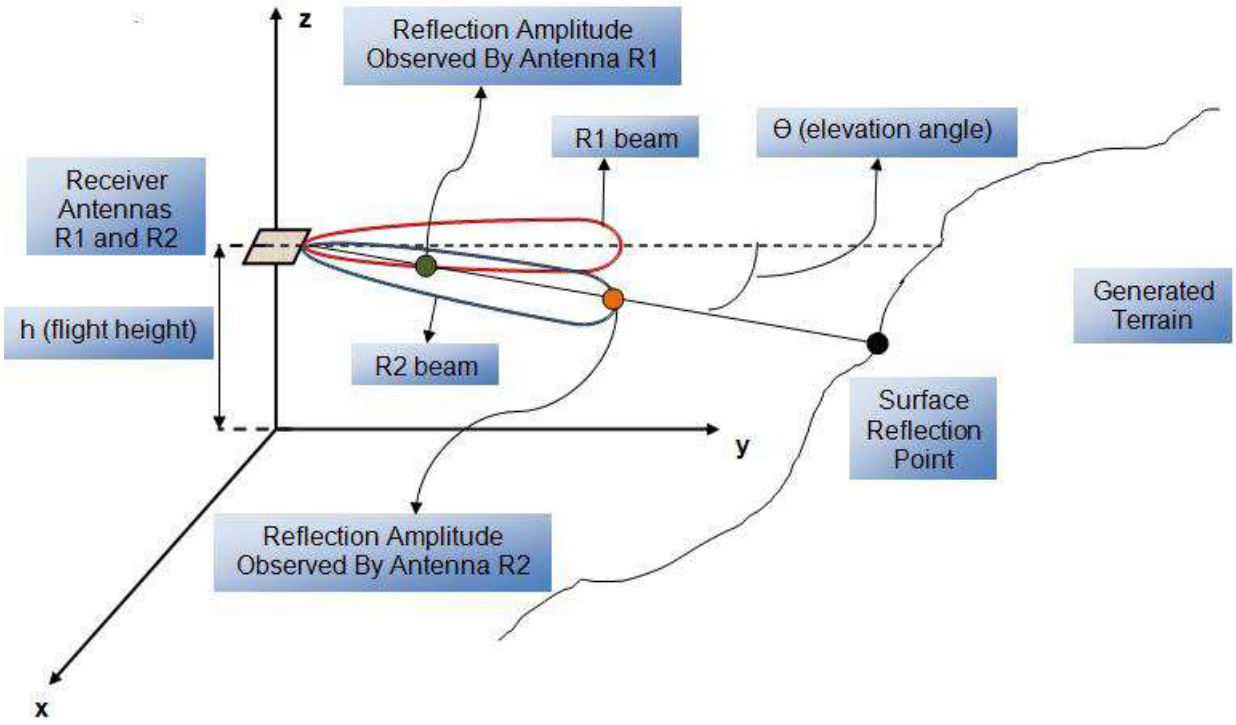

Figure 4.23: Receiver antennas in a scanning pattern.

In angle of arrival based terrain profiling technique, two receiver antennas $R1$ and $R2$ with same antenna pattern are used. $R1$ antenna is looking forward and $R2$ antenna is looking downward with some elevation angle. The elevation angle θ is different for transmitter and receiver antennas, but they have the same angle ϕ in azimuth direction. The transmitter antenna illuminates the synthetic terrain and echoes from the synthetic terrain are received by $R1$ and $R2$ antenna. In Fig. 4.23, the schematic of these receiver antennas that are receiving a reflection from a single patch is shown. As you can see in Fig. 4.23, the amplitude of the reflection from a surface point is different for $R2$ and $R1$ antennas. They received these reflections with different gain values. The logic behind this technique is, trying to obtain elevation angle θ of the reflections by using the ratio of different observed reflection amplitudes $\frac{R2}{R1}$ of $R2$ and $R1$ antennas. Here in Fig. 4.23, the elevation angle θ for a single surface reflection point is shown, and there is a relation between this $\frac{R2}{R1}$ amplitude ratio of the received echoe by $R2$ and $R1$

antennas and the elevation angle θ of the echoe. If this relation is known, then it will be used to find elevation angle θ values of the echoes. By this way, for all echoes, the elevation angle θ can be found and then it's easy to estimate the terrain elevation data from these θ values. Since the technique tries to find the elevation angle θ values of the echoes in the estimation of the terrain profile, it's based on angle of arrival information.

So, we have searched the relation between the received signals ratio by $R2$ and $R1$ antennas and the corresponding elevation angle θ. The received signals received by $R2$ and $R1$ antennas are firstly pulse doppler processed like discussed in chapter 3.3. And then, the clutter received signals for $R2$ and $R1$ antennas are found from the corresponding bin of doppler-range matrix. In finding the relation between the amplitude ratio $\frac{R2}{R1}$ of these clutter received signals and the elevation angle θ, we've put a single surface patch points to a specified range and to the different θ angles which are changing with very small increments. Then, for each patch in different θ angles, raw radar data is generated. By using this raw radar data, the received signals received by $R2$ and $R1$ antenna are generated. And the clutter received signals are generated by using pulse-Doppler processing on the received signals of $R2$ and $R1$ antennas. Thus, the clutter received signal amplitude ratio $\frac{R2}{R1}$ for the corresponding elevation angle θ can be found. By this way, it's formed a look-up table between this amplitude ratio $\frac{R2}{R1}$ and elevation angle θ. In forming this look-up table, θ angles are being changed with very small increments. But for finding the values beside the look-up table, some interpolation is used.

This look-up table is used as reference in the simulations for estimating the terrain profile. In simulations over the synthetic terrain, the raw radar data is generated for $R2$ and $R1$ antennas. Then, the corresponding received signals are formed and they are pulse-Doppler processed. The clutter received signals are obtained from the doppler-range matrix of these pulse-Doppler processed

received signals for both $R2$ and $R1$ antennas. And the ratio between the clutter received signals of $R2$ and $R1$ antenna is calculated for all of the ranges. Fig. 4.24 shows a sample of the clutter received signals for $R2$ and $R1$ antenna and the ratio between them according to the range values. Since we have a look-up table including the relation between θ angle and clutter received signal amplitude ratio $\frac{R2}{R1}$, it's easy to find the corresponding θ elevation angles for the ratio values in different ranges. If a ratio value is among the two ratio values in look-up table, the θ angle corresponding to it is found by interpolating θ angles of those two ratio values. Then, for all ratio values the corresponding θ angles are found as shown in Fig. 4.24. So, we have θ angles over the corresponding range values. Now, we can find the corresponding height values for all ranges by using some geometrical calculations. Since the flight height and the θ angles of the echoes are known, the height of the echoe in the corresponding range can be found like in Eq. (4.6).

$$h(R) = H + R.sin(\theta), \tag{4.6}$$

where $h(R)$ is the height value of the clutter in the R range, H is the flight height, R is the range and θ is the elevation angle of the clutter. We take the θ values below the horizon as negative, and the θ values over the horizon as pozitive. Briefly, angle of arrival based terrain profiling technique is based on estimating terrain profile by using the elevation angle information of the echoes. This angle information is found by means of the relation between $\frac{R2}{R1}$ ratio and θ elevation angle. Let's have a look at the results obtained by this technique.

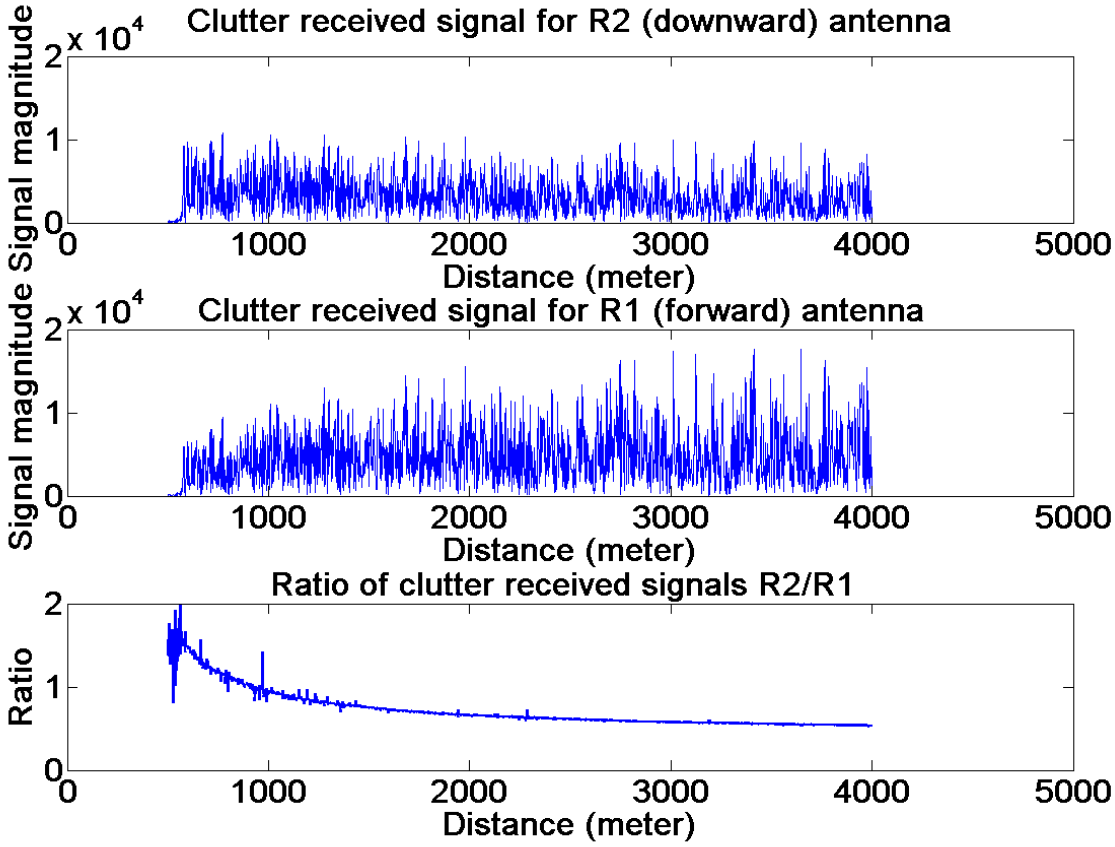

Figure 4.24: The clutter received signal samples for $R2$ and $R1$ antennas and their ratio.

4.2.1 Results

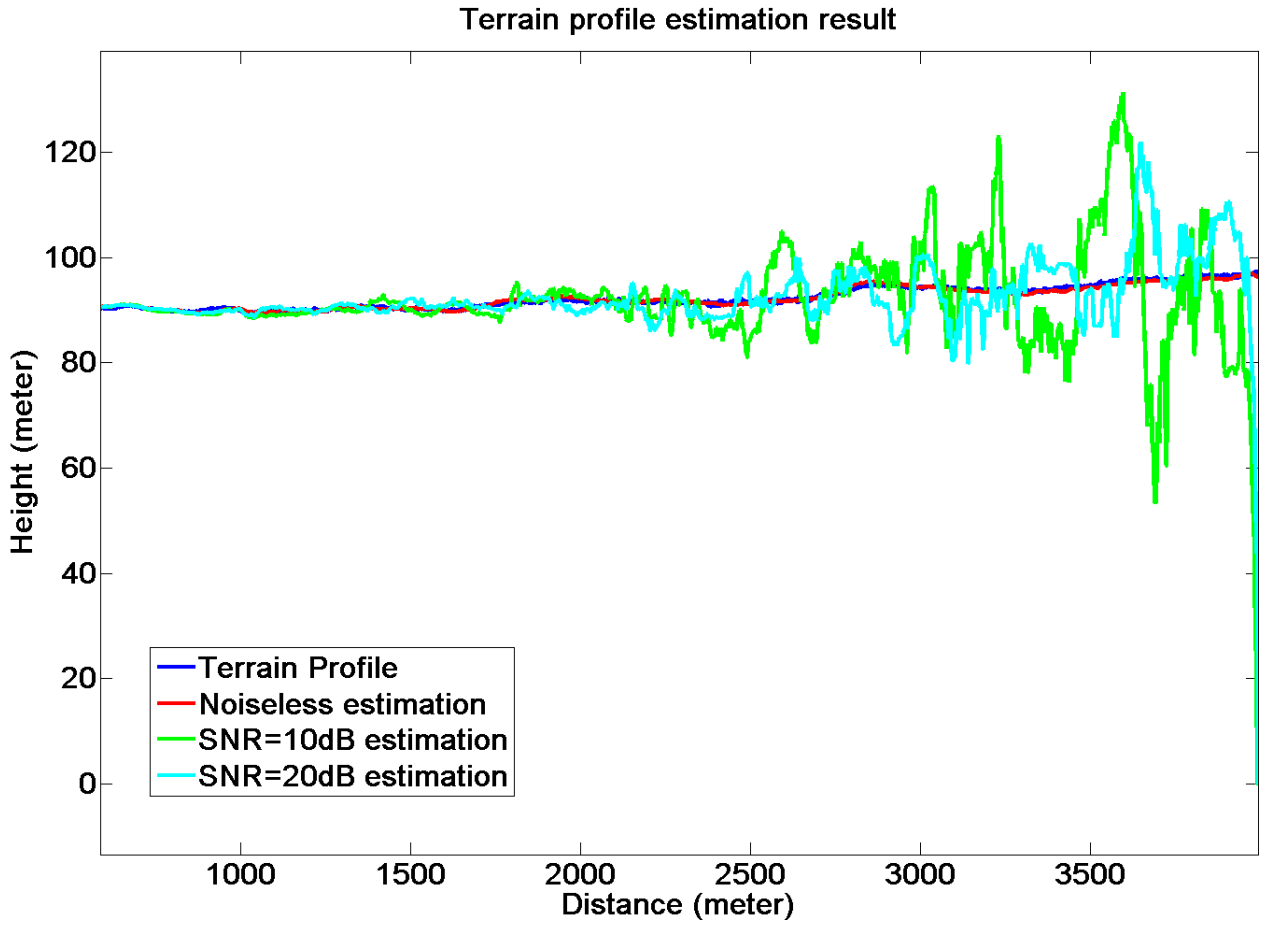

Figure 4.25: The estimation of the terrain profile without noise and with different SNR values.

Here in Fig. 4.25, the estimation results without noise and with SNR values are shown. The synthetic terrain is shown in blue. The red one is the noiseles estimation, the green one is the estimation with 10 dB SNR value and the light blue one is the estimation with 20 dB SNR value. As it can be seen, the noiseless estimation is very similar with the synthetic terrain profile all over the range. Estimations with 10 dB and 20 dB SNR values are still good estimation results. They have some distortions which increase for far ranges. The distortions in far ranges for the 10 dB and 20 dB SNR estimations can be explained as the

big changes in height values through small changes in elevation angle θ. The sensitivity for θ angle in finding the height value increases for far ranges. Small θ angle error causes big height errors in far ranges. Since the noise in 10 dB and 20 dB SNR values affect θ angle and these distortions in far ranges occurs. Though the estimations are said to be good. The noiseless estimation has the best result naturally.

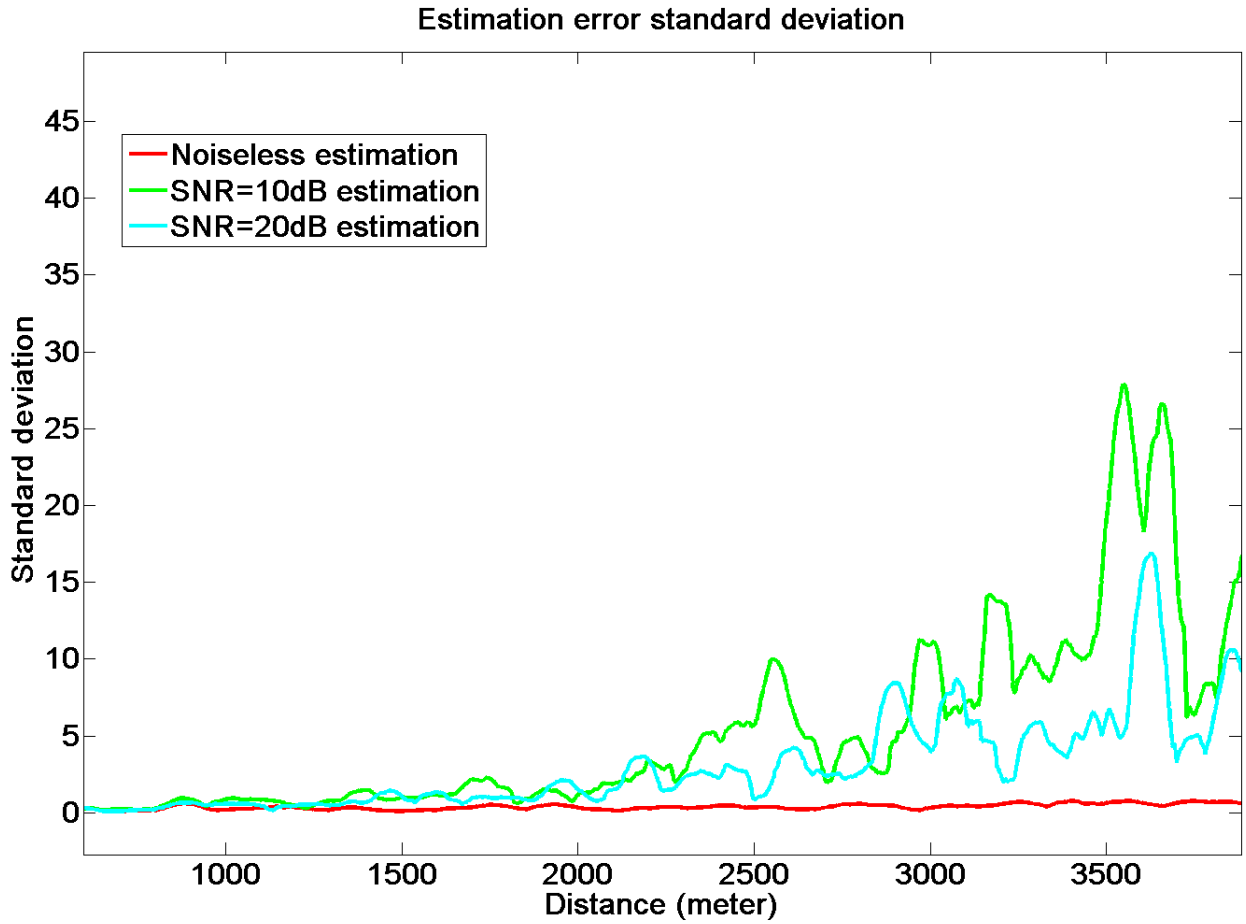

Figure 4.26: The standard deviation of the estimated terrain profiles in Fig. 4.25 according to the range.

Fig. 4.26 is the standard deviation values according to the range for Fig. 4.25. The noiseless estimation has a very little standard deviation from the synthetic terrain. 10 dB and 20 dB SNR estimations has standard deviations smaller than

10 meter until 3000 meter range and has some peak deviations after 3000 meter range. But still they have reasonable and good estimation results for 170 meter flight altitude.

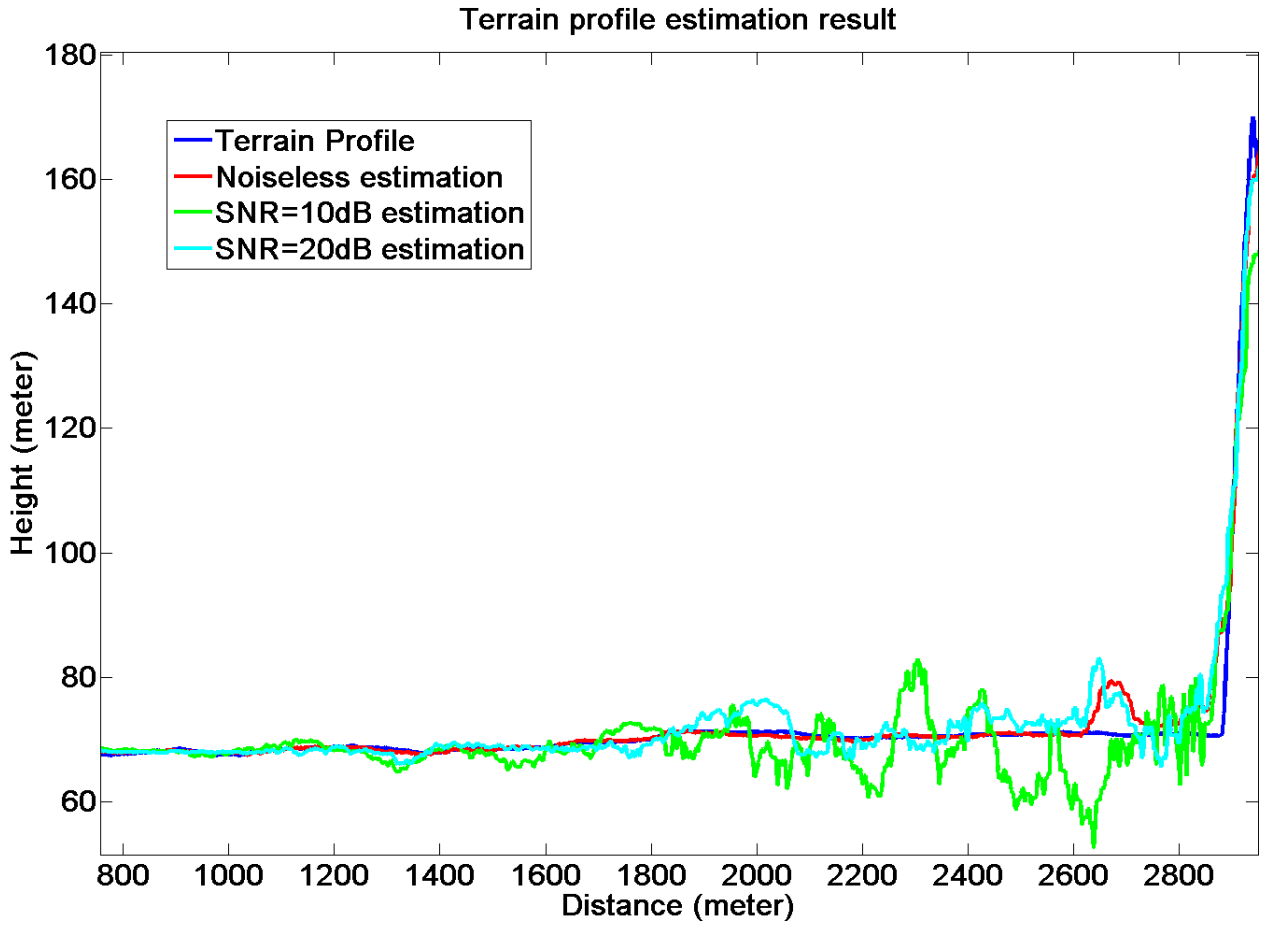

Figure 4.27: The estimation of the terrain profile for a synthetic terrain including a hill, without noise and with different SNR values.

Fig. 4.27 is the estimation results of noiseless, 10 dB and 20 dB SNR values for a synthetic terrain that has a hill. As you can see, there is a hill in altitude of the flight altitude around 2900 meter range. The results are very acceptable for both 10 dB and 20 dB SNR estimations and noiseless estimation. The estimations are very consistent with the synthetic terrain and the hill shape, especially the noiseless estimation.

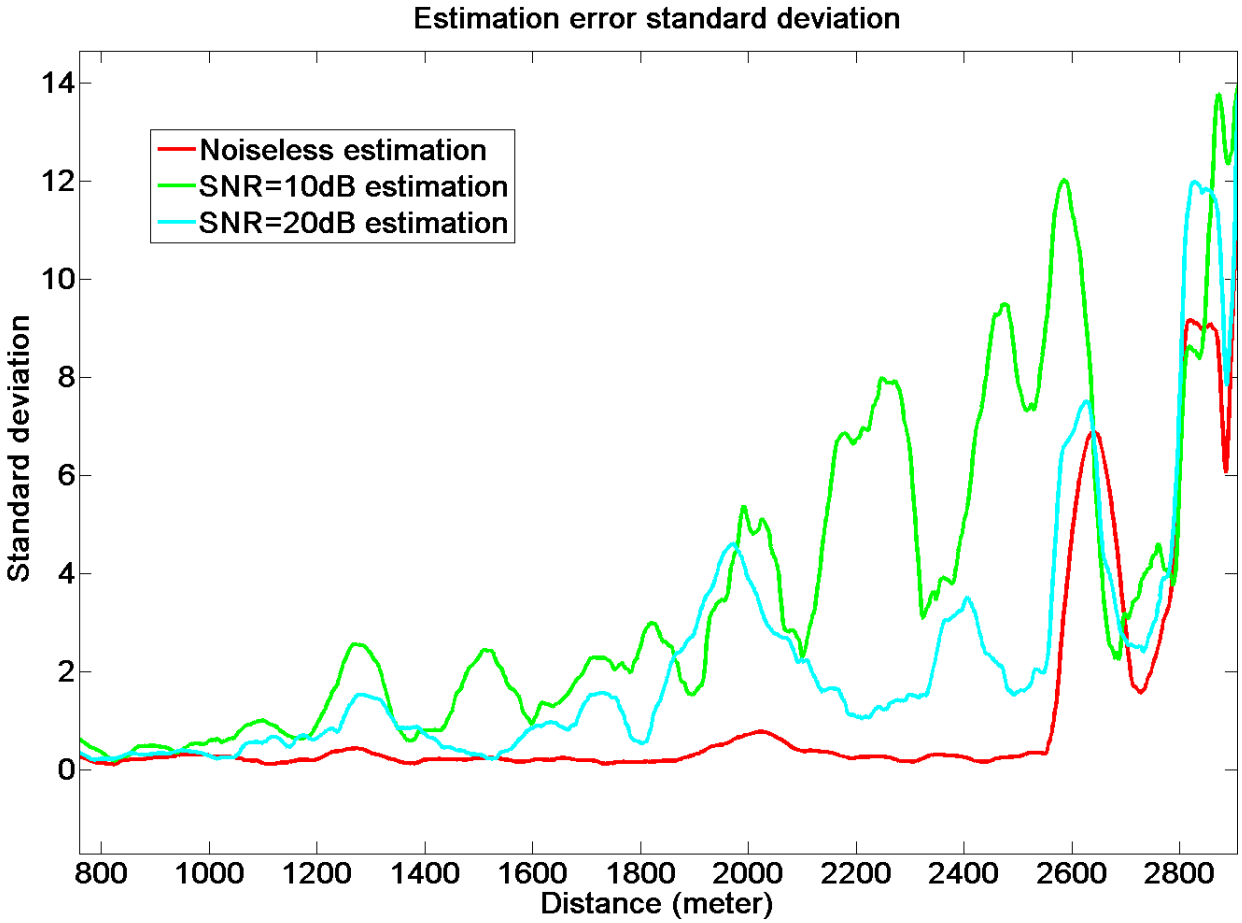

Figure 4.28: The standard deviation of the estimated terrain profiles in Fig. 4.27 according to the range.

Fig. 4.28 is the standard deviation values according to the range for the Fig. 4.27. The standard deviation naturally increases around the hill for three estimation. But it's very reasonable, because the error values are around 10 meter near to the hill for the 170 meter flight altitude. When thinking of a hill in 2900 meter range, this can be thought as a good estimation result. Because the error will get better as the aircraft comes closer to the hill and the pilot has a response time to prevent a crash.

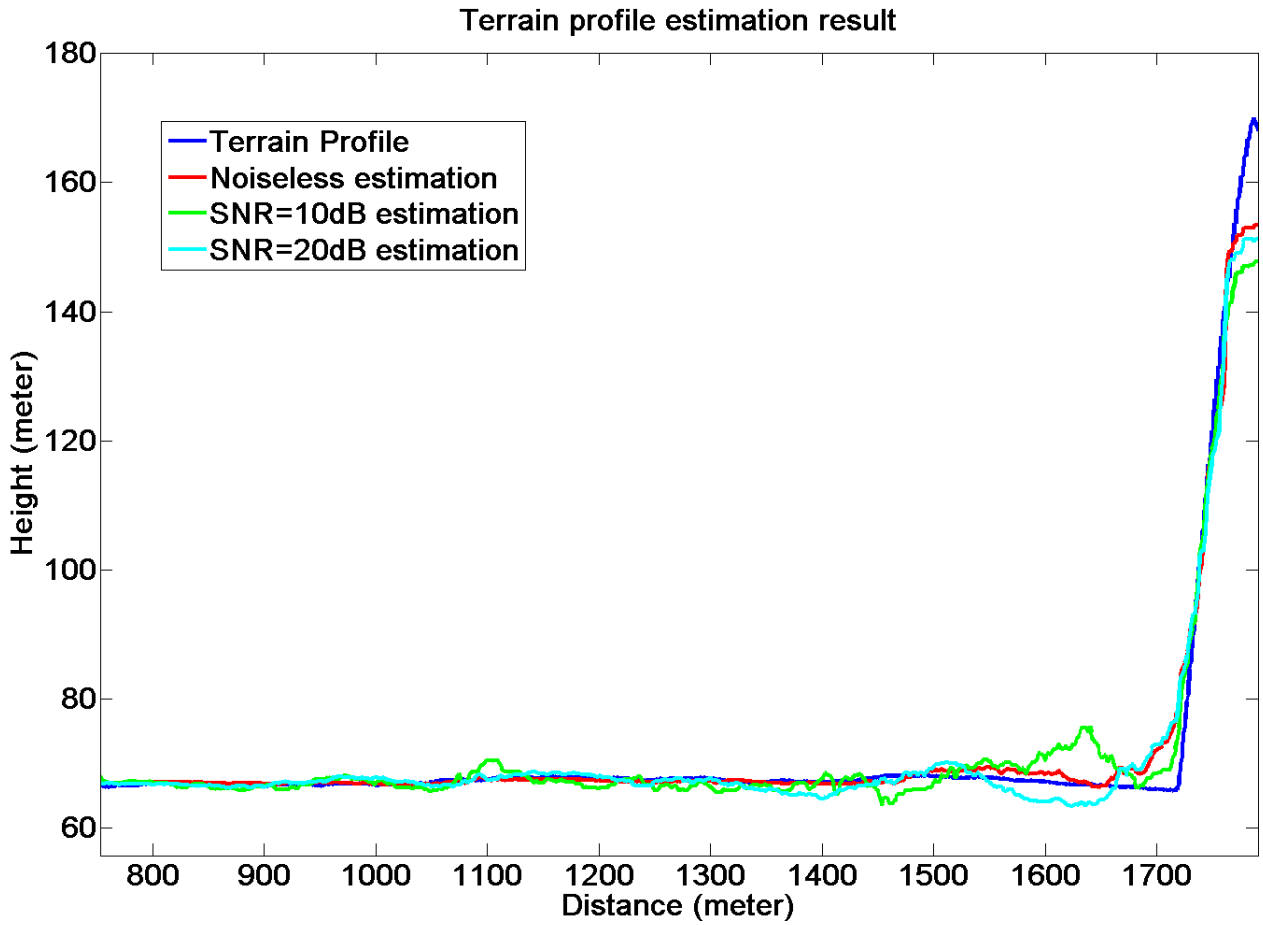

Figure 4.29: The estimation of the terrain profile for a synthetic terrain including a hill, without noise and with different SNR values.

In Fig. 4.29, the estimation results are shown for synthetic terrain including a hill. This time, hill is closer than the hill in Fig. 4.27. It's around 1800 meter range and in altitude of the flight altitude. We can see that the estimations are similar to the synthetic terrain profile. Similarly, before the hill there are some little deviations for three estimations which is not so important. They quickly fit to the synthetic hill shape. All of the estimations follow the shape of the synthetic terrain.

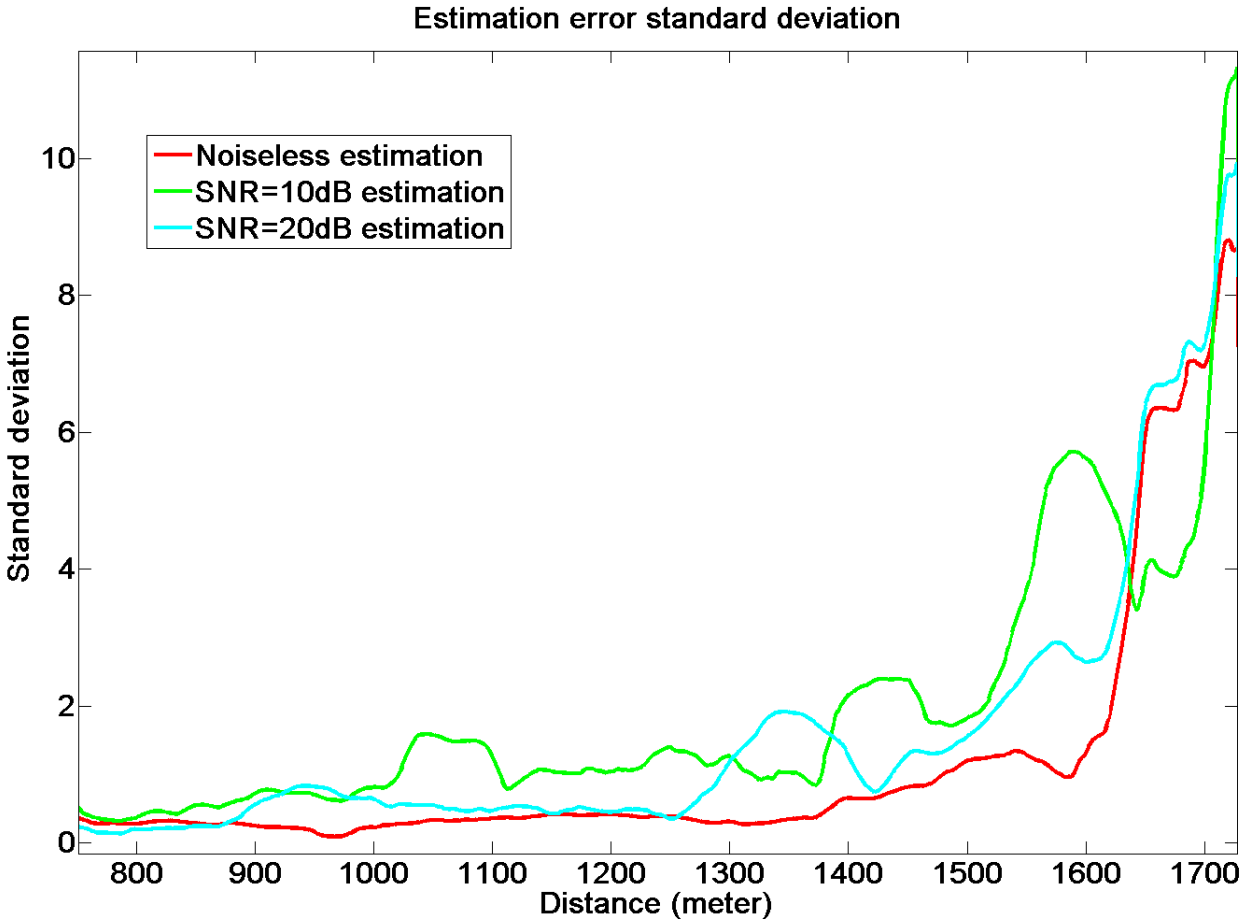

Figure 4.30: The standard deviation of the estimated terrain profiles in Fig. 4.29 according to the range.

Fig. 4.30 is the standard deviation values according to the range for the Fig. 4.29. The standard deviations similarly increases around the hill. Standard deviation values are so reasonable such as 8 meter around the hill. In other ranges rather than the range of the hill, the deviations are very good smaller than 2 meter for three estimations. The synthetic terrain with closer range hill is estimated as the synthetic terrain with far range hill. The shape of the synthetic terrain around hill and other ranges is conserved for all of the estimations. And the errors are very reasonable for all estimations considering the flight altitude of the aircraft.

Angle of arrival based terrain profiling technique is successfully fulfilled as time of arrival based terrain profiling technique. All over the range values, estimations fit to the synthetic terrain shape with reasonable error results. Naturally, noiseless estimation has the best performance. But the performance of 10 dB and 20 dB SNR estimations is also very acceptable. They are very similar to the noiseless estimation in close ranges. Though far ranges, their estimation errors are in reasonable level. The peak deviations in far ranges for 10 dB and 20 dB SNR estimations, are due to the sensivity of the θ angle in finding height value. The small changes in θ angle causes big height differences in finding height values for far ranges. That's why there are some distortions for 10 dB and 20 dB SNR estimations in far ranges. But still these distortions are very acceptable. For synthetic terrain shapes including two hill in different ranges, the estimations are very successful again. They fit to the hill shape. Around the hill, the standard deviation increases in a very reasonable manner considering the flight altitude.

Time of arrival based terrain profiling technique and angle of arrival based terrain profiling technique are both successful in estimating the terrain profile. In time of arrival based terrain profiling technique, there is one antenna behaving as transceiver. On the other hand, angle of arrival based terrain profiling technique has a transmitter antenna and two receiver antennas. Using less antenna is the advantage of time of arrival based terrain profiling technique over angle of arrival based terrain profiling technique. But angle of arrival based terrain profiling technique generates more sensitive and less erroneous terrain profile estimations. It also gets those results in a wider range than time of arrival based terrain profiling technique. They both have advantageous and disadvantageous sides over them. But overall, both techniques give reasonable estimations with good error values.

Chapter 5

CONCLUSION

The systems used in terrain profile estimation become very important in civil transport, in military applications for providing safe flight to the pilot and the crew. In this thesis, the terrain profile estimation of a synthetically generated terrain is obtained using signal processing with two developed techniques. A simulation environment is formed to run the simulations and to observe the estimation performance of the techniques. In the simulations, the synthetic terrain is scanned with an aircraft that has a pulse-Doppler radar mounted on it. The performance of two techniques is compared according to the simulation results.

Time of arrival based terrain profiling technique is the first developed method in estimating the terrain profile. In this technique, the synthetic terrain is scanned with a pencil beam antenna. The technique is based on the usage of time of arrival information of the echoes for the estimation of the terrain profile. It processes the pulse-Doppler processed received signals to find the first and the middle reflection range points and uses them to estimate the terrain profile. The first and the middle reflection range points in clutter received signal are related with the time of arrival of the clutter. For finding the first and the middle reflection ranges in the clutter received signal, an adaptive thresholding algorithm is

developed. In this algorithm, the edges of the clutter received signal is detected and the signal part is seperated from the noise part. We observed rare false detections naturally, due to the usage of adaptive threshold. Since these rare false detections affect the performance of the technique, a way is proposed to prevent them. We observed a high correlation between the first reflection ranges of the neighbour clutter received signals in the same and the consecutive scans. This correlation information helps us to prevent the false detections. From these range points, the transition to the ground coordinates is realized and by using 2D interpolation the estimated terrain profile is obtained. We observed that both the usage of the first and the middle reflection range points has successfully estimated the synthetic terrain profile shape with reasonable error results. The middle reflection range points usage has better performance in mean error values according to the first reflection range points usage. The elevation and the azimuth angle of the antenna's middle beam point is used in the transition to the ground coordinates from the range points. Since the reflection that has come from the antenna's middle beam point illumination area is more probably in the middle reflection range of the clutter received signal rather than the first reflection range, the middle reflection range usage gives better mean error results.

Angle of arrival based terrain profiling technique is the other developed method in estimating the terrain profile. This technique is based on the angle information of the echoes in the estimation of the terrain profile. It uses the relation between the elevation angle θ and the clutter received signal amplitude ratio $\frac{R2}{R1}$ of the two receiver antennas $R1$ and $R2$ to find the elevation angle θ of the clutter in the corresponding range. We generated a look-up table specifying the relation between the clutter received signal amplitude ratio $\frac{R2}{R1}$ and the elevation angle θ of the clutter. By using this look-up table and the amplitude ratio of the clutter received signals, the θ angles of the clutter can be found all over the range. From these θ angles, the estimated height values are found in the corresponding ranges by means of some geometrical calculations. The estimations fit

to the synthetic terrain with very reasonable error results. Noiseless estimation has the best error values as expected. In the synthetic terrain without a hill, the estimation is very good with the deviation 2 meter all over the range. 10 dB and 20 dB SNR estimations have also very reasonable results. There are some peak deviations from the synthetic terrain for far ranges in these 10 dB and 20 dB SNR estimations. The reason is that the small changes in θ angle causes big height differences in finding height values for far ranges. The affect of the noises in 10 dB and 20 dB SNR values in specifying the θ angle for far ranges cause these distortions. But these distortions are in reasonable level. The estimations for synthetic terrains including two hills with an altitude of flight altitude in different ranges, have also fit to the shape of the synthetic terrain around hill and other ranges. The deviations around the hills increase in acceptable borders considering the flight altitude.

To conclude, time of arrival based terrain profiling technique and angle of arrival based terrain profiling technique have succesfully estimated the synthetically generated terrain. There is a trade-off between these techniques. Time of arrival based terrain profiling technique uses less antennas than angle of arrival based terrain profiling technique which is important in total cost of the hardware and mounting of these antennas to the aircraft. Angle of arrival based terrain profiling technique gives better estimation results in a wider range than time of arrival based terrain profiling technique in considering the error values. But in overall, two techniques give reasonable and reliable estimation results in the consequence of the simulations. Our future work will consist of developing the estimations with minimal hardware costs and reflecting those estimations to the pilot cabin for helping the pilot in a best way to prevent the crashes.

Bibliography

[1] J. K. Kuchar, "Markov model of terrain for evaluation of ground proximity warning system thresholds," *Journal Of Guidance, Control and Dynamics*, vol. 24, pp. 430–433, May-June 2001.

[2] W. R. Gilliland and T. A. Nichols, "System and method for enhanced situational awareness of terrain in a vertical situation display," *United States Patent, Honeywell International Inc.*, April 2007.

[3] M. A. Richards, *Fundamentals of Radar Signal Processing.* McGraw Hill, 2005.

[4] G. W. Stimson, *Introduction to Airborne Radar.* SciTech Publishing, 1998.

[5] R. C. Becker and L. D. Almsted, "Flight test evaluation of a 35 ghz forward looking altimeter for terrain avoidance," *IEEE AES Systems Magazine*, February 1995.

[6] B. D., "How to terrain-proof corporate and regional aircraft," *Flight Safety Digest*, vol. 12, no. 8, pp. 38–67, 1993.

[7] B. P.J., "The use of digital map data to provide enhanced navigation and displays for poor weather penetration and recovery," *Journal Of Navigation*, vol. 46, no. 2, pp. 208–222, 1993.

[8] S. J. Kemeny J.G. and, *Finite Markov Chains.* D. Van Nostrand Co. Princeton, NJ, Chapter 3, 1967.

[9] R. Y. Szeto and B. G. Cornell, "Vertical profile display with arbitrary plane," *United States Patent, Honeywell International Inc.*, January 2005.

[10] J. M. Wichgers and J. L. Spicer, "Integrated horizontal and profile terrain display format for situational awareness," *United States Patent, Honeywell International Inc.*, August 1999.

[11] P. R. Frederick, "Automatic horizontal and vertical scanning radar with terrain display," *United States Patent, Honeywell International Inc.*, July 1988.

[12] E. Ma, "Simulating nature," *Project A*, pp. 4–20, June 2002.

[13] H. L. Demko S. and N. B., "Construction of fractal objects with iterated function systems," *ACM*, vol. 19, no. 3, 1985.

[14] M. B.B., "The fractal geometry of nature," *Freeman New York*, 1977.

[15] K. F., "Fractal models of natural phenomena," *SIGGRAPH 01 Simulating Nature Course*, 2001.

[16] P. Martz, "Generating random fractal terrain," *Project*, pp. 1–11.

[17] G. S. Miller, "The definition and rendering of terrain maps," *SIGGRAPH Conference Proceedings,Computer Graphics*, vol. 20, August 1986.

[18] R. D. Voss, "Fractals in nature:characterization,measurement and simulation," *SIGGRAPH Course Notes 15*, 1987.

[19] G. Macklem, "Computer landscape generation and smoothing," *Masters Comprehensive Exam*, pp. 1–8, 2003.

[20] V. P. Joost van Lawick and H. Jense, "Dynamic terrain generation based on multifractal techniques," *In Proceedings of the International Workshop on High Performance Computing for Computer Graphics and Visualisation*, pp. 186–199, 1996.

[21] B. D. Sagar and K. Murphy, "Generation of a fractal landscape using non-linear mathematical morphological transformations," *Fractals*, vol. 8, no. 3, 2000.

[22] R. Krten, "Generating realistic terrain," *Dr. Dobb's Journal:Software Tools for the Professional Programmer*, vol. 19, July 1994.

[23] K. Arakawa and E. Krotkov, "Fractal modelling of natural terrain:analysis and surface reconstruction with range data," *Graphical Models and Image Processing*, September 1996.

[24] D. F. Alain Fournier and L. Carpenter, "Computer rendering of stochastic models," *Communications of the ACM*, vol. 25, pp. 371–384, June 1982.

[25] A. Dewdney, "Computer recreations:of fractal mountains, graftal plants and other computer graphics at pixar," *Scientific American*, December 1986.

[26] J. R. Moss, "Fractal terrain generation system specification," May 1997.

[27] D. Doo and M. Sabin, "Behaviour of recursive division surfaces near extraordinary points," *Computer Aided Design*, vol. 10, no. 6, pp. 356–360, 1978.

[28] M. I. Skolnik, *Introduction to Radar Systems.* McGraw Hill, 2001.

[29] G. R. Curry, "A global perspective of affordable radar systems for the new millennium, radar system performance modelling," *IEEE 2005 International Radar Conference, Tutorial J*, pp. 23–31, May 2005.

[30] N. Levanon, "A global perspective of affordable radar systems for the new millennium, radar waveforms:analysis and design," *IEEE 2005 International Radar Conference, Tutorial H*, pp. 4–10, May 2005.